

Thermocapillary instability of a surfactant-laden shear-imposed film flow

Arnab Choudhury  and Arghya Samanta **Department of Applied Mechanics, Indian Institute of Technology Delhi, 110016 Delhi, India*

(Received 8 January 2024; accepted 15 July 2024; published 1 August 2024)

We examine the linear thermocapillary instability of a two-dimensional gravity-driven shear-imposed incompressible viscous film flowing over a uniformly heated inclined wall when the film surface is covered by an insoluble surfactant. The aim is to expand the prior research [Wei, *Phys. Fluids* **17**, 012103 (2005)] to the case of a nonisothermal viscous film. As a result, the energy equation is incorporated into the governing equations along with the mass conservation and momentum equations. In the present study, we have found two additional thermocapillary S- and P-modes in the low to moderate Reynolds number regime, along with the known H-mode (surface mode) and surfactant mode. The long-wave analysis predicts that the surfactant Marangoni number, which measures the surface tension gradient due to a change in insoluble surfactant concentration, has a stabilizing impact on the H-mode, but the thermal Marangoni number, which measures the surface tension gradient due to a change in temperature, has a destabilizing impact. These opposing effects produce an analytical relationship between them for which the critical Reynolds number for the H-mode instability of the nonisothermal film flow coincides with that of the isothermal film flow. On the other hand, the numerical result exhibits that the surfactant Marangoni number has a stabilizing influence on the thermocapillary S-mode and P-mode. More specifically, these thermocapillary instabilities diminish with an increase in the value of the surfactant Marangoni number. However, these thermocapillary instabilities can be made stronger by increasing the value of the thermal Marangoni number. Furthermore, the thermal Marangoni number destabilizes the surfactant mode instability, but the onset of instability is not affected in the presence of the thermal Marangoni number, which is in contrast to the influence of the surfactant Marangoni number on the onset of surfactant mode instability. Interestingly, the Biot number, which measures the ratio of heat convection and heat conduction, shows a dual role in the surfactant mode instability, even though the threshold of instability remains the same. In the high Reynolds number regime, the shear mode appears and is stabilized by the surfactant Marangoni number but destabilized by the thermal Marangoni number. Moreover, the comparison of results with inertia and without inertia exhibits a stabilizing role of inertia in the surfactant mode.

DOI: [10.1103/PhysRevFluids.9.084002](https://doi.org/10.1103/PhysRevFluids.9.084002)

I. INTRODUCTION

Because of their numerous applications in engineering and technology, the studies of interfacial heat transfer and stability in falling liquid films have been of interest to researchers worldwide. Since thin liquid films have a wide contact area and low thermal resistance, they are frequently encountered in a variety of industrial equipment, including falling film evaporators, condensers, etc. [1]. Moreover, liquid films are very useful for the cooling of microelectronic devices, the solidification of liquid metal, and the thermal protection of rocket engines. Additionally, the solitary

*Contact author: arghya@am.iitd.ac.in

wave formation on the surface of a falling film greatly enhances heat and mass transfers, as reported in the works of Frisk and Davis [2] and Brauner and Maron [3]. As a result, the inclusion of heat transfer in the study of isothermal film flows plays an important role in the falling film instability, especially in the development of surface waves downstream generated by the streamwise gravitational force. Unlike the heat transfer phenomenon, the introduction of interfacial surfactant also alters the interfacial properties of the liquid film and boundary conditions, and hence modifies the rates of heat and mass transfers at the liquid-air interface [4]. These facts stimulate us to unravel the combined thermal and surfactant effects on the falling film instability.

Since the seminal experimental work of Kapitza and Kapitza [5], there have been numerous studies of the isothermal thin liquid films devoted to the investigation of linear and nonlinear stability analyses, where they have revealed all the events, including the initiation of primary instability, the nonlinear interaction of primary waves, and the evolution of a single tear-drop-shaped solitary wave (see, for example, [6–8]). In this context, Benjamin [9] and Yih [10] conducted the linear stability of a gravity-driven isothermal thin liquid film flowing on an impermeable substrate at a low Reynolds number based on the Orr-Sommerfeld boundary value problem. They identified the H-mode (surface mode) in the long-wave regime, where they assumed that the film thickness is very small in comparison with the wavelength of the infinitesimal perturbation. The critical Reynolds number for the onset of the H-mode instability was determined as a function of the angle of inclination. In fact, the H-mode arises due to the streamwise component of the gravitational force. After that, the emergence of shear mode instability in the high Reynolds number regime for the isothermal gravity-driven film flow was reported by Lin [11], Bruin [12], and Chin [13]. Bruin showed that the surface mode and the shear mode compete among themselves to control the primary instability when the inclination angle is sufficiently small. Later the effect of surface tension on the shear mode instability was examined by Floryan [14]. In particular, the shear mode and the surface mode are not the same [15]. The shear mode emerges due to the viscous effect when the Reynolds number is very high, but the inclination angle is sufficiently small [13].

In the context of thermocapillary instability, Lin [16] initiated the long-wave linear stability analysis of a nonisothermal falling film on an inclined heated substrate when the Reynolds number is low. For the onset of H-mode instability, he determined the critical Reynolds number. To investigate the thermocapillary instability for disturbances of arbitrary wave numbers, Sreenivasan and Lin [17] further revisited the flow model of Lin for a sufficiently small inclination angle. Later Smith [18] introduced the effect of the Prandtl number on the primary instability of a nonisothermal thin liquid film. To perform the stability analysis, he implemented the long-wave asymptotic expansion. His result revealed that the thin film flow can be unstable to infinitesimal disturbances for large values of the Prandtl number. He also discussed the physical mechanism of primary instability. On the basis of the method of energy budget, Goussis and Kelly [19] rendered an alternative physical mechanism of instability for a nonisothermal thin film flow over a uniformly heated substrate. They identified one hydrodynamic mode (H-mode) and two thermocapillary modes (S-mode and P-mode) for low to moderate values of the Reynolds number, where the S-mode and P-mode arise due to the thermocapillary effect. In particular, the H-mode and the thermocapillary S-mode appear in the long-wave regime, while the thermocapillary P-mode appears in the short-wave regime. As per their discussion, the S-mode and P-mode instabilities, induced by the destabilizing thermocapillary forces, emerge via two distinct physical mechanisms: (1) As the fluid surface deforms due to an infinitesimal disturbance, it causes a modification to the base flow temperature. This fact is responsible for the appearance of the thermocapillary S-mode instability in the long-wave regime. (2) On the other hand, the appearance of the thermocapillary P-mode instability in the finite wave number regime is responsible for the convective interaction between the perturbation velocity field and the basic temperature. Furthermore, Goussis and Kelly [19] reported that the P-mode instability for a nonisothermal film flow will emerge if the following criterion is satisfied:

$$\left[-\frac{d\sigma}{dT} \Delta T \right] \frac{\rho c_p}{\mu \lambda} > 32.073, \quad (1)$$

where σ is the surface tension, ΔT is the difference between the wall temperature and the ambient temperature, ρ is the density, c_p is the specific heat capacity at constant pressure, μ is the dynamic viscosity, and λ is the heat transfer coefficient at the liquid film surface. It should be noted that the expression $[-\frac{d\sigma}{dT}\Delta T]$, created by a change in surface tension due to a change in temperature, represents a measure of the thermocapillary force, while the expression ρc_p represents a measure of the effect of convection in extracting energy from the basic state. Obviously, the large magnitudes of these quantities endorse the appearance of P-mode instability. On the other hand, the dynamic viscosity μ and the heat transfer coefficient λ , respectively, measure the energy loss due to viscous dissipation and heat loss through the fluid surface. Therefore, these two quantities are opposing to cause P-mode instability. Hence, for the emergence of P-mode instability, the energy transfer from the basic state to the disturbance and the work done by the thermocapillary force should be greater than these kinds of energy losses. Moreover, they examined the influence of the thermal Marangoni number on the H-mode, S-mode, and P-mode and reported that the thermal Marangoni number has a destabilizing impact on these dominant unstable modes. Joo *et al.* [20] incorporated the evaporation effect into the studies of heated thin film flow and executed a linear stability analysis based on the long-wave asymptotic expansion. After that, Joo *et al.* [21] further revisited their prior work in exploring the nonlinear stability based on the evolution equation for the liquid film thickness. As mentioned by them, the rivulet formation is generated due to the thermocapillary S-mode instability. To decipher the complex wave dynamics on the surface of a nonisothermal falling film on a heated substrate, Ruyer-Quil *et al.* [22] and Scheid *et al.* [23] carried out the instability analysis in detail under the framework of low-dimensional modeling. As a result, they developed three evolution equations in terms of the local film thickness, local flow rate, and mean temperature across the layer. The steady-state traveling wave solution was computed numerically. They showed that the results obtained from the low-dimensional model are in good agreement with those of the Orr-Sommerfeld boundary value problem. Moreover, they recognized the hydrodynamic H-mode and the thermocapillary S-mode instabilities, which reinforce each other as the thermal Marangoni number increases. Hu *et al.* [24] accomplished a linear stability analysis for the nonisothermal binary liquid film flowing over a heated substrate. They analyzed the influence of the Soret number on the H-mode, S-mode, and P-mode in a low to moderate Reynolds number regime. These unstable modes are destabilized as the Soret number rises. Moreover, they revealed an interesting phenomenon: the H-mode and S-mode merge for the higher values of the Soret number. Pascal and D'Alessio [25] and D'Alessio and Pascal [26] took the same flow model as Hu *et al.* [24] to examine the linear and nonlinear stability analyses based on the Orr-Sommerfeld-type boundary value problem and depth-averaged equations. After that, D'Alessio *et al.* [27] conducted a study on the Marangoni instability for a heated falling film in the presence of soluble surfactant. Again, both linear and nonlinear stability analyses were performed. Their results predicted that the surfactant Marangoni number has a stabilizing effect, but the thermal Marangoni number has a destabilizing effect on the H-mode. Furthermore, they showed that the results of insoluble surfactant can be recovered in the limiting case. Samanta [28] investigated the impacts of the thermal Marangoni number and the Biot number on the temporal instability in the limit of inertialess approximation for the nonisothermal film flow over a uniformly heated substrate. He showed that the Biot number has a destabilizing role in the H-mode instability. On the basis of the Benney-type surface evolution equation, Dávalos-Orozco [29] performed a nonlinear stability analysis of a heated liquid film over an impermeable substrate. He analyzed the effects of wall thickness and heat conductivity on the H-mode instability. A thorough review of isothermal and nonisothermal thin film flows can be found in the study of Dávalos-Orozco [30]. Recently, a detailed study on the thermocapillary instability of a thin film flowing over a uniformly heated slippery substrate was provided by Choudhury and Samanta [31]. They reported the existence of an additional shear mode when the Reynolds number is high. They also revealed that wall slip destabilizes the thermocapillary P-mode instability but stabilizes the shear mode instability. Furthermore, they showed that the spanwise wave number has a destabilizing influence on the thermocapillary P-mode instability. After that, Choudhury and Samanta [32] investigated the thermocapillary instability for a shear-imposed nonisothermal film

flow. They showed that the H-mode and S-mode instabilities are destabilized, but the P-mode instability is stabilized if the shear stress is imposed in the coflow direction. Furthermore, the onset of instability for the H-mode and the onset of stability for the S-mode coalesce and produce a single onset for the primary stability as the shear stress increases. However, an opposite phenomenon occurs if the shear stress is applied in the counterflow direction. In addition, they demonstrated that the shear mode instability is weakened if the shear stress is acting in the counterflow direction.

On the other hand, the studies of hydrodynamic instability for insoluble surfactant-laden flows are of particular interest as the change in surfactant concentration imparts a variation in surface tension at the interface, which in turn triggers and affects some important instability mechanisms. In this context, the study of the linear stability of a falling film containing soluble and insoluble surfactants was originated by Whitaker and Jones [33], and they predicted the critical Reynolds number for the surfactant-laden film flow to become unstable. Later Blyth and Pozrikidis [34] extended the flow model of Whitaker and Jones up to a moderate Reynolds number regime and reported a stabilizing effect of insoluble surfactant on the dominant unstable H-mode. After that, Wei [35] introduced a constant shear stress at the surface of a thin film flow when it is contaminated by an insoluble surfactant. He developed the Orr-Sommerfeld-type boundary value problem to investigate the primary instability in the long-wave regime. He stated that the surfactant mode emerges due to the presence of surface surfactant and becomes unstable if the shear stress is imposed in the coflow direction. The flow model of Wei was further revisited by Bhat and Samanta [36] to unravel the shear mode instability in the high Reynolds number regime. They revealed that the surfactant Marangoni number stabilizes the shear mode instability. The Marangoni instability of two-layer film flow with insoluble surfactant was analyzed by Frenkel and Halpern [37] in the inertialess limit. Including inertia, Samanta [38] extended the study of Frenkel and Halpern up to a moderate Reynolds number regime and predicted that the presence of interfacial surfactant stabilizes the interfacial mode at high viscosity ratio but destabilizes it at low viscosity ratio.

Clearly, the above literature survey on heated film flows without surfactant demonstrates that the thermal Marangoni number destabilizes the H-mode, S-mode, and P-mode instabilities. On the other hand, the literature survey on surfactant-laden film flows reveals that the surfactant Marangoni number has a stabilizing impact on the H-mode instability. However, there is no study devoted to exploring the combined effect of the thermal Marangoni number and the surfactant Marangoni number on the H-mode, S-mode, P-mode, shear mode, and surfactant mode simultaneously in the presence of imposed shear stress. For this reason, we are motivated to carry out a linear stability analysis of a shear-imposed insoluble surfactant-laden thin film flowing down a heated substrate, where the heated substrate is maintained at a constant temperature. In this study we have deciphered the effects of several parameters like the thermal Marangoni number, the Biot number, and the surfactant Marangoni number on the H-mode, S-mode, P-mode, shear mode, and surfactant mode, respectively. We have organized our paper in the following way: Sec. II concerns the problem description along with the governing equations. Section III discusses the derivation of the Orr-Sommerfeld-type boundary value problem (OS BVP) with its long-wave analytical solution. The numerical solution of the OS BVP for an arbitrary Reynolds number as well as the current numerical results are provided in Sec. IV. Section V deals with the linear stability analysis in the inertialess approximation. Finally, we have presented the summary and conclusions in Sec. VI. In addition, we have briefly discussed the thermocapillary instability of a liquid film with a soluble surfactant in the presence of an imposed shear stress in Appendix. The details are kept for future investigation.

II. GOVERNING EQUATIONS

The present study consists of a two-dimensional flow of viscous incompressible liquid film falling down an inclined wall due to gravitational force. Suppose the inclined wall makes an angle θ with the horizontal. The flow configuration is schematically depicted in Fig. 1. The mathematical equations are developed based on the Cartesian coordinate system, where the origin is placed on the

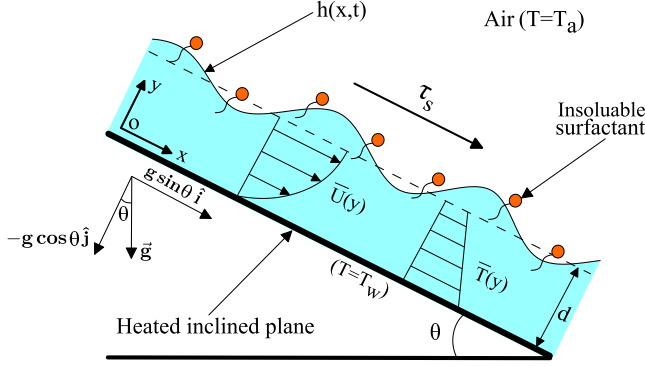


FIG. 1. Schematic diagram of a thin viscous liquid film falling down a uniformly heated inclined wall with inclination angle θ in the presence of a constant shear stress τ_s . Here d is the height of the unperturbed film flow, and $h(x, t)$ is the height of the perturbed film flow. Furthermore, $\bar{U}(y)$ and $\bar{T}(y)$, respectively, represent the velocity and temperature profiles of the base flow. Here $\bar{g} = g \sin \theta \hat{i} - g \cos \theta \hat{j}$ is the gravity acceleration vector, and \hat{i} and \hat{j} are unit vectors along x axis and y axis, respectively.

wall and the axes x and y are directed along the wall and normal to the wall, respectively. In this study, we have considered a set of assumptions: (1) The liquid film surface is contaminated by a layer of insoluble surfactant with concentration $\Gamma(x, t)$. (2) A constant shear stress, τ_s , is imposed along the streamwise flow direction. If $\tau_s > 0$, the shear stress is applied in the coflow direction. Otherwise, it is applied in the counterflow direction if $\tau_s < 0$. (3) The bounded wall is uniformly heated with a temperature of $T = T_w$, which is higher than the ambient temperature $T = T_a$. (4) As we intend to examine the thermocapillary instability, the surface tension $\sigma(T, \Gamma)$ is considered to be a function of both temperature T and surfactant concentration Γ , and it will be varied by the following linear relation [27,39,40]:

$$\sigma(T, \Gamma) = \sigma_a - \beta(T - T_a) - E(\Gamma - \Gamma_a), \quad (2)$$

where σ_a is the base surface tension at the base surfactant concentration Γ_a when $T = T_a$. Here $\beta = -d\sigma/dT|_{T=T_a} > 0$ and $E = -d\sigma/d\Gamma|_{\Gamma=\Gamma_a} > 0$, as surface tension decreases with the increase in the values of both temperature and surfactant concentration. (5) The other thermophysical properties of the nonisothermal liquid film, like density ρ , dynamic viscosity μ , specific heat capacity c_p , and thermal conductivity κ , are considered constants throughout the study. The heights of the unperturbed and perturbed liquid films are denoted by d and $h(x, t)$, respectively. The flow dynamics of the two-dimensional nonisothermal liquid film and the heat transfer within the liquid film are governed by the following mass conservation, momentum, and energy equations [41–43]:

$$\partial_x u + \partial_y v = 0, \quad (3)$$

$$\rho(\partial_t u + u\partial_x u + v\partial_y u) = -\partial_x p + \mu(\partial_{xx} u + \partial_{yy} u) + \rho g \sin \theta, \quad (4)$$

$$\rho(\partial_t v + u\partial_x v + v\partial_y v) = -\partial_y p + \mu(\partial_{xx} v + \partial_{yy} v) - \rho g \cos \theta, \quad (5)$$

$$\rho c_p(\partial_t T + u\partial_x T + v\partial_y T) = \kappa(\partial_{xx} T + \partial_{yy} T), \quad (6)$$

where u , v , p , and T are, respectively, the streamwise velocity component, cross-stream velocity component, pressure, and temperature of the nonisothermal liquid film. Here $g = |\bar{g}|$ is the magnitude of the gravity acceleration vector. The current flow configuration is completed by the following boundary conditions: (1) At the tilted heated wall, $y = 0$, the streamwise and cross-stream velocity components must satisfy the no-slip and no-penetration boundary conditions, but the temperature is

constant on the wall. Accordingly, we can write

$$u = 0, \quad v = 0, \quad T = T_w, \quad \text{at } y = 0, \quad (7)$$

where T_w is the temperature at the tilted heated wall. (2) At the liquid-air interface, $y = h(x, t)$, the tangential stress and the normal stress are balanced by the imposed shear stress and the stress induced by the surface tension gradients due to changes in temperature and surfactant concentration, which yield the following dynamic boundary conditions [27,31,32,39]:

$$\mu\{4\partial_y v \partial_x h + (\partial_y u + \partial_x v)[1 - (\partial_x h)^2]\} + [\beta(\partial_x T + \partial_x h \partial_y T) + E \partial_x \Gamma - \tau_s] \sqrt{1 + (\partial_x h)^2} = 0, \quad (8)$$

$$P_a - p + \frac{2\mu}{[1 + (\partial_x h)^2]} \{\partial_y v [1 - (\partial_x h)^2] - \partial_x h (\partial_y u + \partial_x v)\} = \frac{\sigma \partial_{xx} h}{[1 + (\partial_x h)^2]^{3/2}}, \quad (9)$$

where P_a denotes the ambient pressure. (3) At the liquid-air interface, $y = h(x, t)$, the convective heat transfer is governed by Newton's law of cooling [28,41]:

$$\kappa \frac{(\partial_x T \partial_x h - \partial_y T)}{\sqrt{1 + (\partial_x h)^2}} = \lambda(T - T_a), \quad (10)$$

where λ denotes the heat transfer coefficient. (4) The transport of insoluble surfactant concentration at the liquid-air interface, $y = h(x, t)$, is described by the following boundary condition [37,44–46]:

$$\partial_t [\Gamma \sqrt{1 + (\partial_x h)^2}] + \partial_x [\Gamma u \sqrt{1 + (\partial_x h)^2}] = D_s \partial_x [\partial_x \Gamma / \sqrt{1 + (\partial_x h)^2}], \quad (11)$$

where D_s denotes the surfactant diffusivity, which is usually small. (5) Finally, the liquid-air interface, $y = h(x, t)$, evolves with time based on the following kinematic boundary condition:

$$\partial_t h + u \partial_x h = v. \quad (12)$$

A. Nondimensional criterion

The nondimensionalization of the governing equations and associated boundary conditions (3)–(12) is performed by using the following variables with star notation:

$$\begin{aligned} u^* &= \frac{u}{U_s}, & v^* &= \frac{v}{U_s}, & p^* &= \frac{pd}{\mu U_s}, \\ x^* &= \frac{x}{d}, & y^* &= \frac{y}{d}, & h^* &= \frac{h}{d}, & \Gamma^* &= \frac{\Gamma}{\Gamma_a}, \\ t^* &= \frac{t U_s}{d}, & \sigma^* &= \frac{\sigma}{\sigma_a}, & T^* &= \frac{T - T_a}{T_w - T_a}, & \tau &= \frac{\tau_s d}{\mu U_s}, \end{aligned} \quad (13)$$

where $U_s = \rho g d^2 \sin \theta / (2\mu)$ is the base flow velocity at the unperturbed liquid-air interface, $y = d$, in the absence of imposed shear stress. From now on, we have dropped the star notation from the nondimensional variables. The nondimensional governing equations and associated boundary conditions can be expressed as follows:

$$\partial_x u + \partial_y v = 0, \quad (14)$$

$$\text{Re}(\partial_t u + u \partial_x u + v \partial_y u) = -\partial_x p + (\partial_{xx} u + \partial_{yy} u) + 2, \quad (15)$$

$$\text{Re}(\partial_t v + u \partial_x v + v \partial_y v) = -\partial_y p + (\partial_{xx} v + \partial_{yy} v) - 2 \cot \theta, \quad (16)$$

$$\text{Pe}_T(\partial_t T + u \partial_x T + v \partial_y T) = (\partial_{xx} T + \partial_{yy} T), \quad (17)$$

$$u = 0, \quad v = 0, \quad T = 1, \quad \text{at } y = 0, \quad (18)$$

$$\begin{aligned}
 & [4\partial_y v \partial_x h + (\partial_y u + \partial_x v)\{1 - (\partial_x h)^2\}] + [\text{Ma}_T(\partial_x T + \partial_x h \partial_y T) \\
 & + \text{Ma}_S \partial_x \Gamma - \tau] \sqrt{1 + (\partial_x h)^2} = 0, \quad \text{at } y = h,
 \end{aligned} \tag{19}$$

$$\begin{aligned}
 p_a - p + \frac{2}{[1 + (\partial_x h)^2]} [\partial_y v \{1 - (\partial_x h)^2\} - \partial_x h (\partial_y u + \partial_x v)] \\
 = [\text{Ca}^{-1} - \text{Ma}_T T - \text{Ma}_S (\Gamma - 1)] \frac{\partial_{xx} h}{[1 + (\partial_x h)^2]^{3/2}}, \quad \text{at } y = h,
 \end{aligned} \tag{20}$$

$$\frac{(\partial_x T \partial_x h - \partial_y T)}{\sqrt{1 + (\partial_x h)^2}} = \text{Bi } T, \quad \text{at } y = h, \tag{21}$$

$$\partial_t [\Gamma \sqrt{1 + (\partial_x h)^2}] + \partial_x [\Gamma u \sqrt{1 + (\partial_x h)^2}] = \frac{1}{\text{Pe}_S} \partial_x [\partial_x \Gamma / \sqrt{1 + (\partial_x h)^2}], \quad \text{at } y = h, \tag{22}$$

$$\partial_t h + u \partial_x h = v, \quad \text{at } y = h, \tag{23}$$

where $p_a = \frac{P_a d}{\mu U_s}$ denotes the nondimensional ambient pressure, $\text{Re} = \rho U_s d / \mu$ specifies the Reynolds number, which represents the ratio of inertia and the viscous force, $\text{Ma}_T = \beta(T_w - T_a) / \mu U_s$ specifies the thermal Marangoni number, which represents the ratio of the Marangoni force generated by the surface tension gradient due to a change in temperature and the viscous force, $\text{Ma}_S = E \Gamma_a / \mu U_s$ is the surfactant Marangoni number, which represents the ratio of the Marangoni force generated by the surface tension gradient due to a change in surfactant concentration and the viscous force, $\text{Ca} = \mu U_s / \sigma_a$ specifies the capillary number, which represents the ratio of the viscous force and the surface force due to surface tension σ_a , $\text{Bi} = \lambda d / \kappa$ specifies the Biot number, which represents the ratio of the heat convection at the liquid film surface and the heat conduction within the liquid film, $\text{Pe}_S = U_s d / D_s$ specifies the surfactant Péclet number, which represents the ratio of the advective mass transport and the diffusive mass transport at the liquid film surface, and $\text{Pe}_T = \rho c_p U_s d / \kappa = \text{Pr } \text{Re}$ specifies the thermal Péclet number, where $\text{Pr} = \rho c_p \nu / \kappa$ denotes the thermal Prandtl number. We have also introduced the Kapitza number $\text{Ka} = 2\sigma_a / [\rho (v^4 g \sin \theta)^{1/3}] = (2\text{Re})^{2/3} \text{Ca}^{-1}$ to compare our numerical results with those available in the literature, where $\nu = \mu / \rho$ denotes the kinematic viscosity. To decipher the linear stability of the steady unidirectional parallel flow with a constant film thickness, which is also known as the base flow, we require its solution. We have determined the analytical solution of the base flow, which can be expressed as

$$\bar{U}(y) = (2 + \tau)y - y^2, \quad \bar{V}(y) = 0, \quad 0 \leq y \leq 1, \tag{24}$$

$$\bar{P}(y) = 2 \cot \theta (1 - y) + p_a, \quad \bar{H} = 1, \quad 0 \leq y \leq 1, \tag{25}$$

$$\bar{T}(y) = 1 - \left(\frac{\text{Bi}}{1 + \text{Bi}} \right) y, \quad \bar{\Gamma} = 1, \quad 0 \leq y \leq 1, \tag{26}$$

where \bar{H} is the nondimensional height of the base flow and $\bar{\Gamma}$ is the nondimensional surfactant concentration. Clearly, we can observe that the base velocity $\bar{U}(y)$ is a linear function of the imposed shear stress τ but a quadratic function of y . As a result, the base velocity has a semiparabolic form in y , and it increases monotonically as the imposed shear stress increases. Furthermore, the base flow temperature $\bar{T}(y)$ is a linear function of y and also depends on the Biot number Bi . Here we see that the base flow temperature decreases linearly from the wall temperature as we move towards the film surface.

B. Perturbation equations

In this subsection we will derive the linearized perturbation equations. Thereby, we superpose an infinitesimal disturbance on the flat film flow of thickness $\bar{H} = 1$. To describe this phenomenon

mathematically, we decompose each perturbation flow variable in the following form:

$$u = \bar{U} + u', \quad v = \bar{V} + v', \quad p = \bar{P} + p', \quad T = \bar{T} + T', \quad h = \bar{H} + h', \quad \Gamma = \bar{\Gamma} + \Gamma', \quad (27)$$

where u' , v' , p' , T' , h' , and Γ' represent the perturbation flow velocities in x and y directions, perturbation pressure, perturbation temperature, perturbation surface deformation, and perturbation surfactant concentration, respectively. Here the quantities with bar notation represent the base flow variables. Next, the above perturbation decompositions (27) are inserted into the nondimensional governing equations and associated boundary conditions (14)–(23) and linearized those equations with respect to the base flow solutions. Finally, we obtain the following perturbation equations:

$$\partial_x u' + \partial_y v' = 0, \quad 0 \leq y \leq 1, \quad (28)$$

$$\text{Re}(\partial_t u' + \bar{U} \partial_x u' + v' D\bar{U}) = -\partial_x p' + (\partial_{xx} u' + \partial_{yy} u'), \quad 0 \leq y \leq 1, \quad (29)$$

$$\text{Re}(\partial_t v' + \bar{U} \partial_x v') = -\partial_y p' + (\partial_{xx} v' + \partial_{yy} v'), \quad 0 \leq y \leq 1, \quad (30)$$

$$\text{Pe}_T(\partial_t T' + \bar{U} \partial_x T' + v' D\bar{T}) = (\partial_{xx} T' + \partial_{yy} T'), \quad 0 \leq y \leq 1, \quad (31)$$

$$u' = 0, \quad v' = 0, \quad T' = 0, \quad \text{at } y = 0, \quad (32)$$

$$D^2 \bar{U} h' + \partial_y u' + \partial_x v' + \text{Ma}_T[\partial_x T' + D\bar{T} \partial_x h'] + \text{Ma}_S \partial_x \Gamma' = 0, \quad \text{at } y = 1, \quad (33)$$

$$-p' - D\bar{P} h' + 2[\partial_y v' - D\bar{U} \partial_x h'] = (\text{Ca}^{-1} - \text{Ma}_T \bar{T}) \partial_{xx} h', \quad \text{at } y = 1, \quad (34)$$

$$\partial_y T' + \text{Bi}(D\bar{T} h' + T') = 0, \quad \text{at } y = 1, \quad (35)$$

$$\partial_t \Gamma' + \bar{U} \partial_x \Gamma' + \partial_x u' + D\bar{U} \partial_x h' = \frac{1}{\text{Pe}_S} \partial_{xx} \Gamma', \quad \text{at } y = 1, \quad (36)$$

$$\partial_t h' + \bar{U} \partial_x h' = v', \quad \text{at } y = 1, \quad (37)$$

where $D = \frac{d}{dy}$ represents the differential operator.

III. ORR-SOMMERFELD-TYPE EQUATION

To develop the Orr-Sommerfeld-type equation, the perturbation stream function $\psi'(x, t)$ is introduced by using the following relationships:

$$u'(x, t) = \partial_y \psi', \quad v'(x, t) = -\partial_x \psi'. \quad (38)$$

Next, the solution of the perturbation equations (28)–(37) is considered in the form of normal mode [31,47]:

$$\left. \begin{aligned} \psi'(x, y, t) &= \hat{\phi}(y) \exp[i(kx - \omega t)], \\ T'(x, y, t) &= \hat{T}(y) \exp[i(kx - \omega t)], \\ \Gamma'(x, t) &= \hat{\Gamma} \exp[i(kx - \omega t)], \\ h'(x, t) &= \hat{h} \exp[i(kx - \omega t)], \end{aligned} \right\} \quad (39)$$

where $\hat{\phi}(y)$, $\hat{T}(y)$, $\hat{\Gamma}(y)$, and \hat{h} are the amplitudes of the perturbation stream function, perturbation temperature, perturbation surfactant concentration, and perturbation film surface, respectively. Here k and $\omega = kc$ denote the wave number and angular frequency of the infinitesimal perturbation, where c is the wave speed. Next, we will substitute the normal mode solution into the perturbation

equations (28)–(37) and eliminate the pressure terms, which lead to the following form of the Orr-Sommerfeld-type boundary value problem:

$$(D^2 - k^2)^2 \hat{\phi} = ik \operatorname{Re}[(\bar{U} - c)(D^2 - k^2) - D^2 \bar{U}] \hat{\phi}, \quad 0 \leq y \leq 1, \quad (40)$$

$$(D^2 - k^2) \hat{T} = ik \operatorname{Pe}_T [(\bar{U} - c) \hat{T} - D \bar{T} \hat{\phi}], \quad 0 \leq y \leq 1, \quad (41)$$

$$\hat{\phi} = 0, \quad \hat{T} = 0, \quad D \hat{\phi} = 0, \quad \text{at } y = 0, \quad (42)$$

$$(D^2 + k^2) \hat{\phi} + ik \operatorname{Ma}_T (\hat{T} + D \bar{T} \hat{\eta}) + ik \operatorname{Ma}_S \hat{\Gamma} + D^2 \bar{U} \hat{\eta} = 0, \quad \text{at } y = 1, \quad (43)$$

$$\begin{aligned} (D^3 - 3k^2 D) \hat{\phi} - ik \operatorname{Re}[(\bar{U} - c) D \hat{\phi} - D \bar{U} \hat{\phi}] \\ = ik \hat{\eta} [k^2 (\operatorname{Ca}^{-1} - \operatorname{Ma}_T \bar{T}) - D \bar{P} - 2ik D \bar{U}], \quad \text{at } y = 1, \end{aligned} \quad (44)$$

$$D \hat{T} + \operatorname{Bi} [\hat{T} + D \bar{T} \hat{\eta}] = 0, \quad \text{at } y = 1, \quad (45)$$

$$D \hat{\phi} + \left[(\bar{U} - c) - \frac{ik}{\operatorname{Pe}_S} \right] \hat{\Gamma} + D \bar{U} \hat{\eta} = 0, \quad \text{at } y = 1, \quad (46)$$

$$\hat{\phi} + (\bar{U} - c) \hat{\eta} = 0, \quad \text{at } y = 1. \quad (47)$$

To carry out the temporal stability analysis, we will consider that the angular frequency, $\omega = \omega_r + i\omega_i$, is complex while the wave number k is real. Therefore, the wave speed, $c = c_r + ic_i$, is complex.

A. Long-wave analytical solution of the Orr-Sommerfeld-type equation

To investigate the temporal stability analysis in the long-wave regime ($k \ll 1$), we will follow the mathematical technique proposed by Yih [10]. As a result, the variables $\hat{\phi}$, \hat{T} , $\hat{\eta}$, $\hat{\Gamma}$, and c are expanded as the sum of infinite series in the limit $k \rightarrow 0$

$$\left. \begin{aligned} \hat{\phi}(y) &= \sum_{n=0}^{\infty} \phi_n k^n, & \hat{T}(y) &= \sum_{n=0}^{\infty} T_n k^n, \\ \hat{\eta} &= \sum_{n=0}^{\infty} \eta_n k^n, & \hat{\Gamma} &= \sum_{n=0}^{\infty} \Gamma_n k^n, & c &= \sum_{n=0}^{\infty} c_n k^n, \end{aligned} \right\} \quad (48)$$

where n is a non-negative integer. In general, long-wave analysis shows the appearance of H-mode (surface mode) and surfactant mode for the isothermal surfactant-laden film flow [35,36]. To differentiate them, we will use the subscript notations s and m in the subsequent calculations for the H-mode and surfactant mode, respectively. It should be fruitful to point out that the long-wave series expansion (48) is valid in the limit $k \rightarrow 0$. Hence, we can capture only the long-wave unstable modes using the series expansion (48). As soon as k increases, the long-wave series expansion will diverge. Therefore, the unstable modes that appear in the finite wave number regime cannot be determined analytically by using the long-wave series expansion. To find out the unstable modes in the arbitrary wave number regime, we have used the numerical technique discussed in Sec. IV.

B. Zeroth-order approximation

Inserting equation (48) into the Orr-Sommerfeld-type boundary value problem (40)–(47), we collect the leading-order or zeroth-order [$O(k^0)$] equations:

$$D^4 \phi_0(y) = 0, \quad D^2 T_0(y) = 0, \quad 0 \leq y \leq 1, \quad (49)$$

$$\phi_0(y) = 0, \quad T_0(y) = 0, \quad D \phi_0(y) = 0, \quad \text{at } y = 0, \quad (50)$$

$$D^2\phi_0(y) + D^2\bar{U}(y)\eta_0 = 0, \quad D^3\phi_0(y) = 0, \quad \text{at } y = 1, \quad (51)$$

$$DT_0(y) + \text{Bi } T_0(y) + \text{Bi } D\bar{T}(y)\eta_0 = 0, \quad \text{at } y = 1, \quad (52)$$

$$D\phi_0(y) + [\bar{U}(y) - c_0]\Gamma_0 + D\bar{U}(y)\eta_0 = 0, \quad \text{at } y = 1, \quad (53)$$

$$\phi_0(y) + [\bar{U}(y) - c_0]\eta_0 = 0, \quad \text{at } y = 1. \quad (54)$$

After solving the zeroth-order equations (49)–(52), we get

$$\phi_0(y) = \eta_0 y^2 \quad \text{and} \quad T_0(y) = \frac{\text{Bi}^2 \eta_0 y}{(1 + \text{Bi})^2}. \quad (55)$$

It is noticed that the zeroth-order solution $\phi_0(y)$ does not depend on the imposed shear stress τ , and the zeroth-order temperature $T_0(y)$ depends only on the Biot number Bi. Next, with the aid of the zeroth-order kinematic boundary condition (54), one can easily get the zeroth-order phase speed c_0 of the infinitesimal disturbance:

$$c_0 = c_{0s} = (2 + \tau), \quad (56)$$

provided $\eta_0 \neq 0$. Then, by substituting the expression of $c_0 (= c_{0s})$ in the zeroth-order transport equation (53), one can obtain the zeroth-order amplitude of the perturbation surfactant concentration:

$$\Gamma_0 = (2 + \tau)\eta_0. \quad (57)$$

As $\eta_0 \neq 0$, this mode is generated due to the deflection of the liquid film surface from the flat film solution $\bar{H} = 1$, and for this reason, we can call it the H-mode (surface mode) [10]. However, if $\eta_0 = 0$, we cannot use the zeroth-order kinematic boundary condition (54) because it vanishes automatically. Instead, we use the zeroth-order surfactant transport equation (53), which introduces another mode in the flow configuration due to perturbation of the surfactant concentration from its base solution $\bar{\Gamma} = 1$, which is called the surfactant mode [35]. The zeroth-order phase speed of the surfactant mode is

$$c_{0m} = (1 + \tau), \quad (58)$$

provided $\Gamma_0 \neq 0$. The above result indicates that the surfactant mode travels at the same speed as the fluid at the surface of a unidirectional parallel flow if $\eta_0 = 0$. Moreover, it is evident that the zeroth-order phase speed of the H-mode is greater than that of the surfactant mode. Hence, from the leading-order approximation, one can conclude that the H-mode propagates faster than the surfactant mode.

C. First-order approximation

Now our aim is to solve the first-order [$O(k)$] equations, and therefore, we collect the equations containing only first-order terms:

$$D^4\phi_1(y) + i \text{Re}[D^2\bar{U}(y)\phi_0(y) + [c_0 - \bar{U}(y)]D^2\phi_0(y)] = 0, \quad 0 \leq y \leq 1, \quad (59)$$

$$D^2T_1(y) + i \text{Pe}_T\{D\bar{T}(y)\phi_0(y) + [c_0 - \bar{U}(y)]T_0(y)\} = 0, \quad 0 \leq y \leq 1, \quad (60)$$

$$\phi_1(y) = 0, \quad T_1(y) = 0, \quad D\phi_1(y) = 0, \quad \text{at } y = 0, \quad (61)$$

$$D^2\phi_1(y) + i \text{Ma}_T\{T_0(y) + D\bar{T}(y)\eta_0\} + i \text{Ma}_S\Gamma_0 + D^2\bar{U}(y)\eta_1 = 0, \quad \text{at } y = 1, \quad (62)$$

$$D^3\phi_1(y) + i \text{Re}\{[c_0 - \bar{U}(y)]D\phi_0(y) + D\bar{U}(y)\phi_0(y)\} + i D\bar{P}(y)\eta_0 = 0, \quad \text{at } y = 1, \quad (63)$$

$$DT_1(y) + \text{Bi}[T_1(y) + D\bar{T}(y)\eta_1] = 0, \quad \text{at } y = 1, \quad (64)$$

$$D\phi_1(y) - [c_0 - \bar{U}(y)]\Gamma_1 - (c_1 + i/\text{Pe}_S)\Gamma_0 + D\bar{U}(y)\eta_1 = 0, \quad \text{at } y = 1, \quad (65)$$

$$\phi_1(y) - [c_0 - \bar{U}(y)]\eta_1 - c_1\eta_0 = 0, \quad \text{at } y = 1. \quad (66)$$

In the long-wave analysis, we assume that the nondimensional numbers like Re , Ca , Pe_T , Ma_S , Ma_T , Bi , and Pe_S are of order $O(1)$. After solving the first-order equations (59)–(64) using *Mathematica*, we obtain the expressions of $\phi_1(y)$ and $T_1(y)$ in the following forms:

$$\phi_1(y) = \frac{i}{60(1 + \text{Bi})^2} [a_2 y^2 + a_3 y^3 + a_4 y^4 + a_5 y^5], \quad (67)$$

$$T_1(y) = -\frac{i \text{Bi} y}{60(1 + \text{Bi})^3} [b_1 + b_2 y^2 + b_3 y^3 + b_4 y^4], \quad (68)$$

where

$$a_0 = 3\{\text{Bi} \eta_0 \text{Ma}_T - (1 + \text{Bi})^2 [2(\eta_0 \cot \theta + i \eta_1) + \text{Ma}_S \Gamma_0]\},$$

$$a_1 = -\eta_0(1 + \text{Bi})^2(2 + \tau - 3c_0),$$

$$a_2 = 10(a_0 + a_1 \text{Re}),$$

$$a_3 = 20(1 + \text{Bi})^2 \eta_0 \cot \theta,$$

$$a_4 = -5\text{Re}(1 + \text{Bi})^2 c_0 \eta_0,$$

$$a_5 = \text{Re}(1 + \text{Bi})^2(2 + \tau)\eta_0,$$

$$b_1 = 60i \text{Bi}(1 + \text{Bi})\eta_1 + \eta_0 \text{Pe}_T \{20 + 2\text{Bi}[25 + 6\text{Bi} - 5(3 + \text{Bi})c_0] + 5\text{Bi} \tau(4 + \text{Bi})\},$$

$$b_2 = 10\text{Bi}(1 + \text{Bi})c_0 \eta_0 \text{Pe}_T,$$

$$b_3 = -5(1 + \text{Bi})[1 + \text{Bi}(3 + \tau)]\eta_0 \text{Pe}_T,$$

$$b_4 = 3\text{Bi}(1 + \text{Bi})\eta_0 \text{Pe}_T.$$

Next, inserting the expressions of $\phi_1(y)$ and $T_1(y)$ in the first-order surfactant transport equation (65) and the first-order kinematic boundary condition (66), we obtain the algebraic equations in terms of the variables η_0 , η_1 , Γ_0 , and Γ_1 :

$$\begin{aligned} & i\{30(1 + \text{Bi})^2 \text{Ma}_S \Gamma_0 - 30\text{Bi} \text{Ma}_T \eta_0 + (1 + \text{Bi})^2 [(18 - 25c_0)\text{Re} + 60i + 40 \cot \theta + 9\text{Re} \tau]\eta_0\} \\ & - 30(1 + \text{Bi})^2 \{\Gamma_0(c_1 + i/\text{Pe}_S) - \Gamma_1(c_0 - 1 - \tau) - \tau \eta_1\} \\ & + \frac{i}{2} [(10c_0 - 6)\text{Re} - 20 \cot \theta - 3\text{Re} \tau]\eta_0\} = 0, \end{aligned} \quad (69)$$

$$\begin{aligned} & 60(1 + \text{Bi})^2 [(1 + \tau - c_0)\eta_1 - c_1\eta_0] - i\{30\text{Ma}_S \Gamma_0(1 + \text{Bi})^2 - 30\text{Bi} \text{Ma}_T \eta_0 \\ & + (1 + \text{Bi})^2 [(18 - 25c_0)\text{Re} + 60i + 40 \cot \theta + 9\text{Re} \tau]\eta_0\} = 0. \end{aligned} \quad (70)$$

Now for the H-mode (surface mode), we must have $\eta_0 \neq 0$. Using the expressions of c_{0s} ($= c_0$) and Γ_0 , we have determined the expression of c_{1s} for the H-mode:

$$c_{1s} = \frac{i}{30} (d_0 + d_1 \text{Re} + d_2 \cot \theta), \quad (71)$$

$$\Gamma_1 = (e_0 + e_1 \text{Re} + e_2 \cot \theta), \quad (72)$$

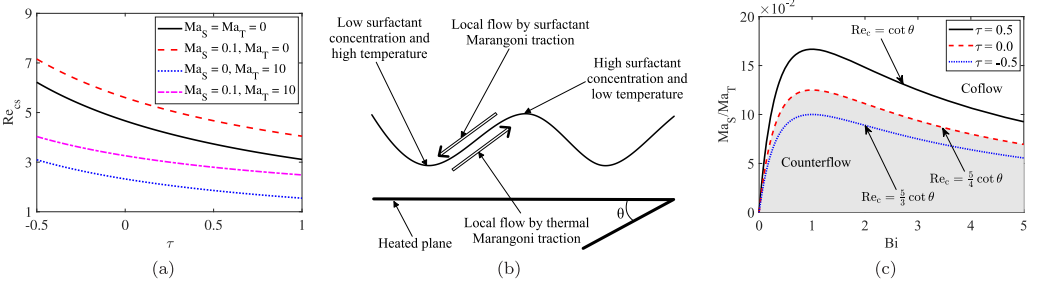


FIG. 2. (a) Variation of the critical Reynolds number Re_{cs} for the H-mode (surface mode) when the imposed shear stress τ varies. Solid, dashed, dotted, and dash-dotted lines represent the results for isothermal ($Ma_S = Ma_T = 0$), surfactant ($Ma_S = 0.1, Ma_T = 0$), thermal ($Ma_S = 0, Ma_T = 10$), and thermal-surfactant ($Ma_S = 0.1, Ma_T = 10$) film flows, respectively. The other parameter values are $Ca = 10, \theta = 15^\circ$, and $Bi = 1$. (b) Schematic diagram of a physical mechanism for the H-mode instability. (c) Variation of $\frac{Ma_S}{Ma_T}$ with the Biot number Bi when τ changes.

where

$$d_0 = 15 \left[\frac{Ma_T Bi}{(1 + Bi)^2} - Ma_S(2 + \tau) \right], \quad d_1 = 8(2 + \tau), \quad d_2 = -20,$$

$$e_0 = \eta_1(2 + \tau) - \frac{i\eta_0}{2} \left\{ \frac{2(2 + \tau)}{Pe_S} + \tau \left[\frac{Ma_T Bi}{(1 + Bi)^2} - Ma_S(2 + \tau) \right] \right\},$$

$$e_1 = -\frac{1}{60} i\eta_0(2 + \tau)(7 + 16\tau), \quad e_2 = \frac{1}{3} i\eta_0(1 + 2\tau).$$

As the imaginary part of the complex wave speed, $c_i \approx |kc_{1s}|$ in the limit $k \rightarrow 0$, $c_{1s} = 0$ specifies the neutral stability condition, which leads to the critical value of the Reynolds number, Re_{cs} , for the onset of H-mode instability, and it can be read as

$$Re_{cs} = \left[\underbrace{\frac{15}{8} Ma_S}_{\text{Surfactant effect}} + \frac{5}{2(2 + \tau)} \cot \theta - \underbrace{\frac{15}{8} \frac{Bi Ma_T}{(1 + Bi)^2(2 + \tau)}}_{\text{Thermal effect}} \right]. \quad (73)$$

Clearly, the analytical expression of the critical Reynolds number for the onset of H-mode instability coincides with that of Wei [35] and Bhat and Samanta [36] for the isothermal ($Ma_S \neq 0, Ma_T = 0$) surfactant-laden film flowing down an inclined plane in the presence of imposed shear stress at the film surface. This result is depicted in Fig. 2(a) by a dashed line when $Ma_S = 0.1$. Furthermore, it recovers the critical Reynolds number for the H-mode instability of the nonisothermal film flowing down an inclined plane [32,48] in the absence of insoluble surfactant ($Ma_S = 0, Ma_T \neq 0$), which is illustrated by a dotted line in Fig. 2(a) when $Ma_T = 10$. If both the thermal effect and surfactant effect are removed ($Ma_S = 0, Ma_T = 0$), then the critical Reynolds number matches very well that of the isothermal shear-imposed viscous film flow [18], which is demonstrated by a solid line in Fig. 2(a). The above expression (73) indicates that the critical Reynolds number for the H-mode (surface mode) increases with the increasing value of the surfactant Marangoni number Ma_S [34,49], but attenuates with the increasing value of the thermal Marangoni number Ma_T [32,48]. Hence, one can expect a stabilizing influence of the surfactant Marangoni number but a destabilizing influence of the thermal Marangoni number on the H-mode. The combined thermal-surfactant effect ($Ma_S \neq 0, Ma_T \neq 0$) on the onset of H-mode instability is displayed in Fig. 2(a) by a dash-dotted line when $Ma_S = 0.1$ and $Ma_T = 10$. In all cases, the threshold of instability for the H-mode decreases as the imposed shear stress increases, which causes a destabilizing impact if it acts in the coflow

direction. However, the imposed shear stress shows a stabilizing influence on the H-mode if it is applied in the counterflow direction. In addition, we can see that the isothermal viscous film flow with an insoluble surfactant is more stable to infinitesimal disturbances, while the nonisothermal viscous film flow without an insoluble surfactant is more unstable compared to the other three film flows. The physical mechanism for the stabilizing impact of the surfactant Marangoni number and the destabilizing impact of the thermal Marangoni number can be described in the following way: (1) For the H-mode (surface mode), we must have $\eta_0 \neq 0$, and the perturbation surfactant concentration and the fluid surface deformation are in the same phase. As a result, the surfactant concentration is low at the trough but high at the crest of the deformed film surface. This fact generates a local flow from the crest-to-trough direction by the surfactant Marangoni traction and yields a stabilizing impact on the H-mode [34,35,37,44]. (2) In contrast, due to the difference in height of the deformed film surface from the wall, the temperature of the viscous film is maximum at the trough and minimum at the crest. Consequently, surface tension is minimum at the trough and maximum at the crest, which causes a local flow from the trough-to-crest direction on the deformed film surface by the thermal Marangoni traction and causes a destabilizing impact on the H-mode. In simple words, the stabilizing influence of surface tension on the H-mode weakens because the surface tension of the viscous film decreases as the thermal Marangoni number Ma_T increases and exhibits a destabilizing impact on the H-mode compared to the isothermal viscous film flow. The above physical mechanism is further shown schematically in Fig. 2(b). Since the effects of the surfactant Marangoni number and the thermal Marangoni number on the H-mode are opposite, these effects can be nullified if the first and third terms of the expression (73) are equal,

$$\frac{15}{8}Ma_S = \frac{15}{8} \frac{Bi Ma_T}{(1 + Bi)^2(2 + \tau)}, \quad (74)$$

which implies

$$\frac{Ma_S}{Ma_T} = \frac{Bi}{(1 + Bi)^2(2 + \tau)} \Rightarrow \frac{E\Gamma_a}{\beta(T_W - T_a)} = \frac{Bi}{(1 + Bi)^2(2 + \tau)}. \quad (75)$$

In this situation, the critical Reynolds number for the onset of H-mode instability for the nonisothermal viscous film flow becomes

$$Re_{cs} = \frac{5}{2(2 + \tau)} \cot \theta, \quad (76)$$

which coincides with the critical Reynolds number for the shear-imposed isothermal viscous film flow [50,51]. That is, for the change in surface tension due to a change in surfactant concentration, we can create a change in surface tension by a change in temperature, for which the critical Reynolds number for the onset of H-mode instability will be independent of the thermal and surfactant effects. This result is demonstrated in Fig. 2(c) for various values of the imposed shear stress τ . If $\tau = 0$, the dashed line in Fig. 2(c) provides the critical Reynolds number of an isothermal viscous film flow down an inclined plane [10]. If $\tau = 0.5 > 0$, the solid line in Fig. 2(c) supplies the critical Reynolds number of an isothermal viscous film flow down an inclined plane when the imposed shear stress acts in the coflow direction [52]. If $\tau = -0.5 < 0$, the dotted line in Fig. 2(c) supplies the critical Reynolds number of an isothermal viscous film flow down an inclined plane when the imposed shear stress acts in the counterflow direction [52]. Next, if $\theta = \pi/2$, the critical Reynolds number for the H-mode instability vanishes. Hence, in this situation, that is, when the thermal and surfactant effects are nullified, the base flow becomes linearly unstable to any infinitesimal disturbance because $Re_{cs} = 0$ at $\theta = \pi/2$. However, if the thermal and surfactant effects are not canceled, that is, when the first and third terms in the expression (73) are not balancing each other, we have a nonzero

expression of the critical Reynolds number for the surface mode at $\theta = \pi/2$, given by

$$\text{Re}_{cs} = \left[\underbrace{\frac{15}{8} \text{Ma}_S}_{\text{Surfactant effect}} - \underbrace{\frac{15}{8} \frac{\text{Bi Ma}_T}{(1 + \text{Bi})^2 (2 + \tau)}}_{\text{Thermal effect}} \right]. \quad (77)$$

Therefore, if $\frac{\text{Ma}_S}{\text{Ma}_T} > \frac{\text{Bi}}{(1 + \text{Bi})^2 (2 + \tau)}$, there exists a range of the Reynolds number where the infinitesimal disturbance is linearly stable. Otherwise, it will be unstable.

Now, for the surfactant mode, we must have $\eta_0 = 0$, but $\Gamma_0 \neq 0$. With the help of the expression c_{0m} , one can determine c_{1m} and η_1 in the following forms:

$$c_{1m} = i \left[\frac{1}{2} \text{Ma}_S \tau - \frac{1}{\text{Pe}_S} \right], \quad (78)$$

$$\eta_1 = \frac{i}{2} \text{Ma}_S \Gamma_0. \quad (79)$$

Therefore, for an unstable surfactant mode, $c_{1m} > 0$, which implies

$$\text{Pe}_S > \frac{2}{\tau} \frac{1}{\text{Ma}_S} = \text{Pe}_{cm}, \quad (80)$$

where Pe_{cm} represents the critical value of the surfactant Péclet number for the onset of surfactant mode instability. Obviously, the expression of Pe_{cm} captures the results of Wei [35] and Bhat and Samanta [36]. It should be noted that the expression (80) is independent of the Reynolds number Re , the thermal Marangoni number Ma_T , and the Biot number Bi . Hence, the critical value of the surfactant Péclet number will not be affected by Re , Ma_T , and Bi . Furthermore, Eq. (78) indicates that the constant shear stress τ must be positive, or equivalently, it should be applied in the coflow direction for the positive growth rate of the surfactant mode. If the above criterion is fulfilled, the surfactant mode will be linearly unstable to infinitesimal surfactant perturbation once $\text{Pe}_S > \text{Pe}_{cm}$.

D. Second-order approximation

Next, we collect the second-order [$O(k^2)$] equations and solve those equations separately in a similar way as discussed above for the H-mode (surface mode) and surfactant mode. The expressions of c_{2s} for the H-mode and c_{2m} for the surfactant mode can be read as

$$c_{2s} = \frac{1}{5040} \left[f_0 - f_1 \text{Ma}_S + f_2 \text{Ma}_S^2 + f_3 \text{Re} - f_4 \text{Re}^2 + f_5 \cot \theta - f_6 \frac{\text{Bi Ma}_T}{(1 + \text{Bi})^3} \right], \quad (81)$$

$$c_{2m} = \frac{\text{Ma}_S}{12} \left\{ \frac{6(2 + \tau)}{\text{Pe}_S} - 2(1 + 2\tau) \cot \theta + \tau \left[\frac{3\text{Bi Ma}_T}{(1 + \text{Bi})^2} - 3(2 + \tau) \text{Ma}_S \right] \right\}, \quad (82)$$

where

$$f_0 = -3360(3 + \tau),$$

$$f_1 = 2520(2 + \tau)/\text{Pe}_S,$$

$$f_2 = 1260\tau(2 + \tau),$$

$$f_3 = 2100\text{Ma}_S(2 + \tau),$$

$$f_4 = 5(2 + \tau)(256 + 77\tau),$$

$$f_5 = 20[(160 + 49\tau)\text{Re} + 426\text{Ma}_S(1 + 2\tau)],$$

$$f_6 = 42[(1 + \text{Bi})(57 + 60\tau)\text{Re} + (15 - 7\text{Bi} - 5\text{Bi}\tau)\text{Pe}_T + 1260\text{Ma}_S\tau(1 + \text{Bi})].$$

E. Third-order approximation

Next, we solve the third-order [$O(k^3)$] equations for the H-mode (surface mode) and the surfactant mode, respectively. In this case, the expressions of c_{3s} and c_{3m} can be read as

$$c_{3s} = -\frac{i}{129\,729\,600} \left\{ 1287 \left[\frac{1680g_0}{\text{Pe}_S^2} + \frac{\text{Ma}_T g_1}{(1+\text{Bi})^4} + \frac{2100\text{Bi}^2 \text{Ma}_T^2 g_2}{(1+\text{Bi})^5} \right] + 2574 \left[20g_3 + \frac{\text{Ma}_T g_4}{(1+\text{Bi})^3} + \frac{5250\text{Bi}^2 \text{Ma}_T^2}{(1+\text{Bi})^4} \right] \text{Re} + 13 \left[g_5 + \frac{\text{Ma}_T g_6}{(1+\text{Bi})^2} \text{Re}^2 + g_7 \text{Re}^3 \right] \right\}, \quad (83)$$

$$c_{3m} = -\frac{i\text{Ma}_S}{5040(1+\text{Bi})^4 \text{Pe}_S^2} \{ 7[20(1+\text{Bi})^4(h_0 + h_1 \text{Pe}_S^2) + h_2 \text{Ma}_T + 90\text{Bi}^2 \text{Pe}_S^2 \text{Ma}_T^2 \tau] + h_3 \text{Re} \}, \quad (84)$$

where

$$g_0 = [4(5\text{Ca}^{-1} - 18 \cot \theta) \text{Pe}_S^2 + 15\text{Ma}_S^3 \text{Pe}_S^2 \tau(2 + \tau) + 5\text{Ma}_S^2 \text{Pe}_S [\cot \theta \text{Pe}_S(8 + 7\tau) + 3(2 + \tau)((1 - ic_{1s})\tau - 2)] + 10\text{Ma}_S(-3(2 + \tau) + \text{Pe}_S\{6ic_{1s} + \cot \theta + (3ic_{1s} + 2 \cot \theta)\tau - \text{Pe}_S[24 + 6c_{2s} + 4ic_{1s} \cot \theta - 2 \csc^2 \theta + (9 + 3c_{2s} + 2ic_{1s} \cot \theta)\tau\})],$$

$$g_1 = 16\,800\{(\text{Bi}^2(5 + 3\text{Bi}) - 2) + \text{Bi}[-50\,400\text{Ma}_S^2(1 + \text{Bi})^2(1 + \tau) + \text{Pe}_T(280(1 + \text{Bi})(7\text{Bi} - 33) \cot \theta + \text{Pe}_T)5435 - \text{Bi}(2090 + 749\text{Bi}) - 10\tau[254\text{Bi} - 130 + 76\text{Bi}^2 + \text{Bi}(52 + 17\text{Bi})\tau]\} + \{420(1 + \text{Bi})\text{Ma}_S[60(1 + \text{Bi})\tau + \text{Pe}_S(3\text{Pe}_T[8\text{Bi} - 20 + 5(\text{Bi} - 1)\tau] + 20i\{1 + \text{Bi}[7i \cot \theta + 3c_{1s}(2 + \tau)])\}]\}/\text{Pe}_S\},$$

$$g_2 = 12(1 + \text{Bi})\text{Ma}_S - (\text{Bi} - 3)\text{Pe}_T,$$

$$g_3 = 6617 + 448 \csc^2 \theta + 1470\text{Ma}_S^2(2 + \tau)10\tau(422 + 49\tau) + \{7\text{Ma}_S[150(2 + \tau) + \cot \theta \text{Pe}_S(249 + 52\tau)]\}/\text{Pe}_S,$$

$$g_4 = -\text{Bi}[13\,720(1 + \text{Bi}) \cot \theta + 1050(1 + \text{Bi})\text{Ma}_S(28 + 5\tau) + \text{Pe}_T\{3653\text{Bi} - 9605 + (3209\text{Bi} - 3490 + 560\text{Bi}\tau)\tau\}],$$

$$g_5 = -990\text{Ma}_S(2 + \tau)[8522 + \tau(3786 + 385\tau)] - 2 \cot \theta [4\,444\,928 + 11\tau(231\,519 + 25\,400\tau)],$$

$$g_6 = 2475\text{Bi}[2707 + 2\tau(750 + 77)],$$

$$g_7 = 4(2 + \tau)[9\,711\,616 + 13\tau(434\,841 + 54\,800\tau)],$$

$$h_0 = 18(2 + \tau) - 3\text{Pe}_S[3\text{Ma}_S(2 + \tau)(2 + 3\tau) + 2 \cot \theta(5 + 4\tau)],$$

$$h_1 = 9\text{Ma}_S^2 \tau(1 + \tau)(2 + \tau) + 2(2 \cot \theta - 3\tau)(1 + 2\tau) + 6 \cot \theta \text{Ma}_S(1 + \tau(5 + 3\tau)),$$

$$h_2 = 3\text{Bi}(1 + \text{Bi})\text{Pe}_S(120(1 + \text{Bi})(1 + \tau) + \text{Pe}_S\{-20(1 + \text{Bi}) \cot \theta + \tau[-80(1 + \text{Bi}) \cot \theta - 30(1 + \text{Bi})\text{Ma}_S(4 + 3\tau) + \text{Bi} \text{Pe}_T(2 + 5\tau)]\}),$$

$$h_3 = 2(1 + \text{Bi})^4 \text{Pe}_S \{ \cot \theta \text{Pe}_S [11 + 3\tau(10 + 7\tau)] - 21(\text{Ma}_S \text{Pe}_S \tau - 2)(2 + (8\tau + 7)\tau) \}.$$

Finally, we combine the expressions of c_{0s} , c_{1s} , c_{2s} , and c_{3s} to determine the complex wave speed c_s for the H-mode [53]

$$c_s = c_{0s} + kc_{1s} + k^2 c_{2s} + k^3 c_{3s} + O(k^4) = c_{rs} + ic_{is}. \quad (85)$$

Hence, the H-mode will be linearly unstable, and the associated infinitesimal perturbation will grow exponentially with time if $c_{is} > 0$. Next, we combine the expressions of c_{0m} , c_{1m} , c_{2m} , & c_{3m} to

determine the complex wave speed c_m for the surfactant mode [53]

$$c_m = c_{0m} + kc_{1m} + k^2c_{2m} + k^3c_{3m} + O(k^4) = c_{rm} + ic_{im}. \quad (86)$$

In this case, the surfactant mode will be linearly unstable if $c_{im} > 0$.

F. Padé approximation of the long-wave solutions

In an analogous fashion with the works of Lange *et al.* [54] and Pal and Samanta [55], we implement the Padé approximation to improve the accuracy of the long-wave result. Consequently, we express the complex wave speed c_s of the H-mode (surface mode) as a ratio of two polynomials in terms of wave number k ($k \rightarrow 0$),

$$c_s = \frac{p_0 + p_1k + p_2k^2 + \dots + p_ik^i}{1 + q_1k + q_2k^2 + \dots + q_jk^j}, \quad (87)$$

where the unknown coefficients p_0, p_1, \dots, p_i , and q_1, \dots, q_j are computed analytically with the aid of the different order long-wave solutions. First, we have demonstrated the results of the H-mode. In particular, we have plotted the neutral stability curve and the temporal growth rate for the H-mode in Figs. 3(a) and 3(b), respectively. The results are computed from the various order long-wave analytical solutions, the Padé approximation, and the numerical simulation. The numerical scheme used for solving the boundary value problem (40)–(47) is discussed in Sec. IV. Clearly, the result determined from the Padé approximation is more accurate compared to the third-order and fifth-order long-wave analytical solutions when the validation is done with the numerical result. In fact, the Padé approximation result arrests the numerical result in a larger range of wave number than those of the third-order and fifth-order long-wave analytical solutions. The reason can be attributed to the nonconverging long-wave result as the wave number increases. On the other hand, Figs. 3(c) and 3(d) demonstrate the comparison of the neutral curve and temporal growth rate for the surfactant mode, where the results are computed from the third-order and fifth-order long-wave analytical solutions, the Padé approximation, and the numerical simulation, respectively. Again, we can see a similar scenario, i.e., the results obtained from the Padé approximation are more accurate than the third-order and fifth-order long-wave solutions, respectively. Figures 4(a) and 4(b) display the neutral stability curve and temporal growth rate for the surfactant mode when Ma_T varies. These results are produced from the third-order long-wave solution. It is observed that the unstable region bounded by the neutral stability curve magnifies as the thermal Marangoni number increases. However, the critical surfactant Péclet number for the onset of the surfactant mode instability remains the same because it does not depend on the thermal Marangoni number [see also Eq. (80)]. To confirm the above result, we further compute the temporal growth rate for the surfactant mode by choosing a fixed value of the surfactant Péclet number from the unstable zone and illustrate it in Fig. 4(b). It should be noted that the temporal growth rate intensifies with the increase in the value of the thermal Marangoni number. Hence, one can conclude that the thermal Marangoni number Ma_T has a destabilizing effect on the surfactant mode. Physically, at higher values of the thermal Marangoni number, surface tension reduces, which in turn destabilizes the surfactant mode. In addition, the current analytical result recovers the result of Bhat and Samanta [49] very well as soon as the thermal Marangoni number Ma_T is set to zero.

IV. NUMERICAL SOLUTION OF THE ORR-SOMMERFELD-TYPE EQUATION

Now we will solve the Orr-Sommerfeld-type equation numerically for disturbances of arbitrary wave numbers. To this end, we employ the Chebyshev spectral collocation method [56]. First, the boundary value problem (40)–(47) is recast into a generalized matrix eigenvalue problem given by

$$\mathcal{A}\hat{\xi} = \omega\mathcal{B}\hat{\xi}, \quad (88)$$

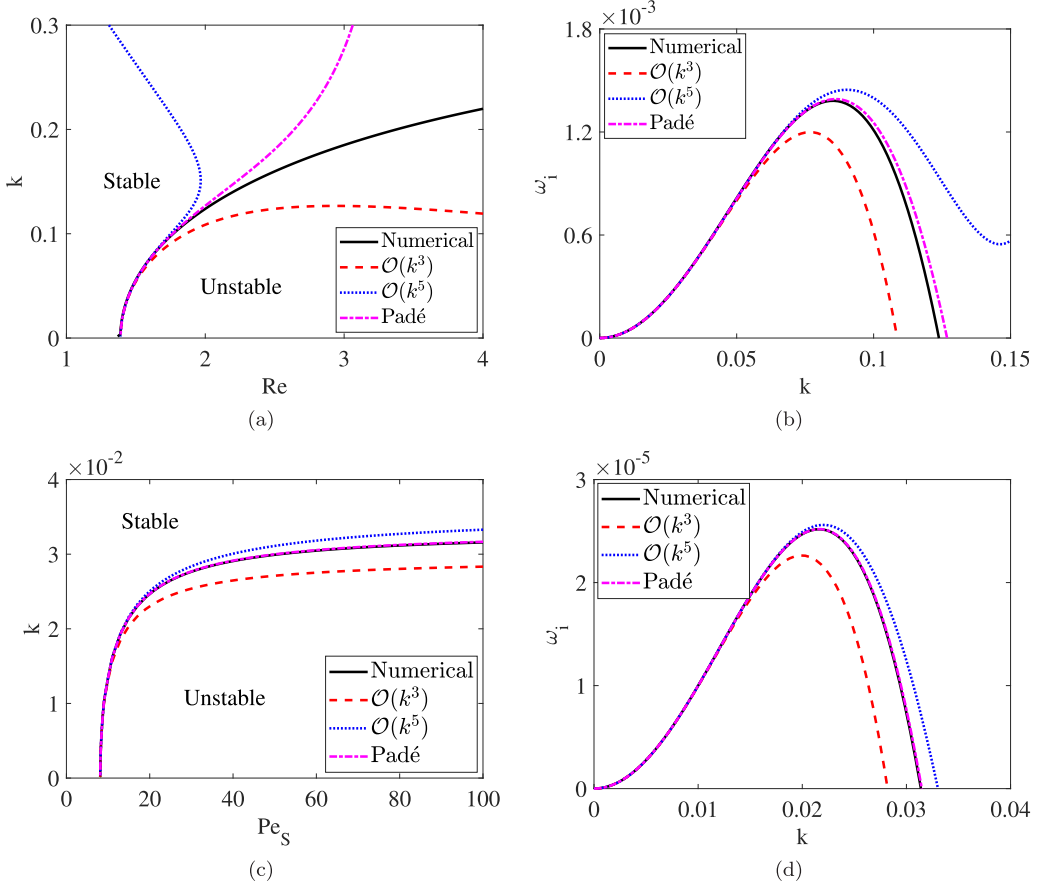


FIG. 3. (a) Comparison of the neutral stability curves in (Re, k) plane for the H-mode (surface mode). (b) Comparison of the associated temporal growth rates in (k, ω_i) plane when $\text{Re} = 2$. The other parameter values are $\text{Ca} = 0.016$, $\text{Pr} = 7$, $\text{Bi} = 1$, $\text{Ma}_T = 25$, $\theta = 15^\circ$, $\tau = 0.5$, $\text{Ma}_S = 1.25$, and $\text{Pe}_S = 1000$. (c) Comparison of the neutral stability curves in (Pe_S, k) plane for the surfactant mode. (d) Comparison of the associated temporal growth rates in (k, ω_i) plane when $\text{Pe}_S = 90$. The other parameter values are $\text{Re} = 20$, $\text{Ca} = 2$, $\text{Pr} = 7$, $\text{Bi} = 1$, $\text{Ma}_T = 10$, $\theta = 3^\circ$, $\tau = 0.5$, and $\text{Ma}_S = 2.5$. Solid, dashed, dotted, and dash-dotted lines stand for the results of the numerical simulation, third-order [$\mathcal{O}(k^3)$] long-wave analytical solution, fifth-order long-wave analytical solution, and the Padé approximation, respectively.

where $\omega = kc$ is the eigenvalue and $\hat{\xi} = [\hat{\phi}, \hat{T}, \hat{\eta}, \hat{\Gamma}]^T$ is the associated eigenvector. The matrices \mathcal{A} and \mathcal{B} can be expressed as follows [51]:

$$\mathcal{A} = \begin{pmatrix} \mathcal{A}_{11} & 0 & 0 & 0 \\ \mathcal{A}_{21} & \mathcal{A}_{22} & 0 & 0 \\ k & 0 & k(1 + \tau) & 0 \\ \mathcal{A}_{41} & 0 & k\tau & \mathcal{A}_{44} \end{pmatrix} \quad \text{and} \quad \mathcal{B} = \begin{pmatrix} \mathcal{B}_{11} & 0 & 0 & 0 \\ 0 & \mathcal{B}_{22} & 0 & 0 \\ 0 & 0 & 1 & 0 \\ 0 & 0 & 0 & 1 \end{pmatrix}, \quad (89)$$

where

$$\begin{aligned} \mathcal{A}_{11} &= k\bar{U}(D^2 - k^2) - kD^2\bar{U} - (D^2 - k^2)^2/(i\text{Re}), \\ \mathcal{A}_{21} &= -kD\bar{T}, \quad \mathcal{A}_{22} = k\bar{U} - (D^2 - k^2)/(i\text{Pe}_T), \end{aligned}$$

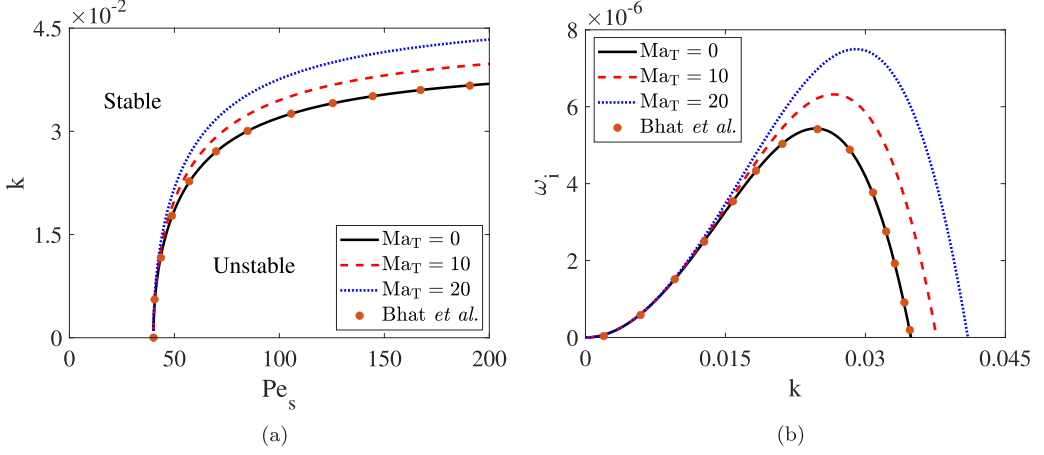


FIG. 4. (a) Variation of the neutral stability curve corresponding to the surfactant mode in (Pe_s, k) plane for different values of the thermal Marangoni number Ma_T when $Re = 4$, $\theta = 4^\circ$, $Ca = 2$, $Pr = 7$, $Bi = 1$, $Ma_S = 0.5$, and $\tau = 0.1$. (b) Associated temporal growth rate in (k, ω_i) plane for different values of Ma_T when $Pe_s = 140$. Solid points are the results of Bhat and Samanta [36].

$$\mathcal{B}_{11} = (D^2 - k^2), \quad \mathcal{B}_{22} = 1, \quad D = \frac{d}{dy},$$

$$\mathcal{A}_{41} = kD, \quad \mathcal{A}_{44} = k(1 + \tau) - ik^2/Pe_s.$$

The last two rows in the matrix eigenvalue problem (88), respectively, represent the evolution of the perturbation film surface deformation and perturbation surfactant transport equations at $y = 1$. The eigenvalue problem is further closed by the remaining boundary conditions (42)–(45). In the Chebyshev spectral collocation method, we expand the amplitude function $\xi(y)$ in a truncated series of the Chebyshev polynomials [47]

$$\xi(y) = \sum_{m=0}^N \xi_m T_m(y), \quad (90)$$

where N is the number of the Chebyshev polynomials. Here ξ_m , ($m = 0, 1, \dots, N$) are unknown Chebyshev coefficients to be determined numerically. Since the Chebyshev polynomials $T_m(y)$ are defined in the interval $[-1, 1]$, the viscous liquid film layer domain $[0, 1]$ is converted to the interval $[-1, 1]$ by using the transformation $y = (x + 1)/2$. Thereby, the derivatives of the flow variables are also converted by the relations $D \rightarrow 2D$, $D^2 \rightarrow 4D^2$, and so on. After substitution of Eq. (90) into the matrix eigenvalue problem (88), the Chebyshev functions $T_m(y)$ are computed at the Gauss-Lobatto collocation points $x_l = \cos(\pi l/N)$, ($l = 0, 1, \dots, N$), which are extrema of the Chebyshev polynomials. Before producing the numerical results, we shall justify our numerical code by comparing its results with the analytical results acquired from the long-wave analysis. Thereby, we compute the critical Reynolds number Re_{cs} for the H-mode (surface mode) as well as the critical surfactant Péclet number Pe_{cm} for the surfactant mode numerically and analytically. Both results are presented in Tables I and II, respectively. We can see that there is an excellent match between the analytical and numerical results. Moreover, the critical Reynolds number for the onset of H-mode instability increases with increasing Ma_S but the critical surfactant Péclet number for the onset of surfactant mode instability decreases with increasing Ma_S . Hence, the surfactant Marangoni number has a stabilizing influence on the H-mode instability but has a destabilizing influence on the surfactant mode instability. As there is a large set of dimensionless numbers, it is difficult to explore their individual effects on the different unstable modes. Moreover, the dimensionless

TABLE I. Comparison between the analytical and numerical values of the critical Reynolds number Re_{cs} for the H-mode (surface mode) when the surfactant Marangoni number Ma_S varies. The other parameter values are $Ca = 0.016$, $\theta = 15^\circ$, $Pr = 7$, $Bi = 1$, $Ma_T = 25$, $Pe_S = 1000$, and $\tau = 0.5$.

| Ma_S | Analytical value (Re_{cs}) | Numerical value (Re_{cs}) |
|--------|--------------------------------|-------------------------------|
| 1.2500 | 1.3883 | 1.3826 |
| 1.5625 | 1.9742 | 1.9791 |
| 1.8750 | 2.5602 | 2.5648 |
| 2.1875 | 3.1461 | 3.1454 |
| 2.5000 | 3.7321 | 3.7356 |

numbers Ma_S , Ma_T , and Bi depend on the physical properties of the nonisothermal surfactant-laden liquid as well as the thickness of the unperturbed liquid layer. Therefore, our aim is to construct dimensionless groups that are dependent only on the physical properties of the nonisothermal surfactant-laden liquid at a given inclination angle θ . Based on the study of Goussis and Kelly [19], we have the following reduced set of relevant flow parameters: $M_T = Ma_T(2Re)^{2/3} = \frac{2\beta(T_w - T_a)}{\rho[g \sin \theta v^4]^{1/3}}$, $M_S = Ma_S(2Re)^{2/3} = \frac{2E \Gamma_a}{\rho(g \sin \theta v^4)^{1/3}}$, and $B = Bi/(2Re)^{1/3} = \frac{\lambda v^{4/3}}{\kappa (g \sin \theta)^{1/3}}$, where M_T , M_S , and B can be called the modified thermal Marangoni number, the modified surfactant Marangoni number, and the modified Biot number, respectively. Clearly, the new dimensionless groups M_T , M_S , and B are independent of the thickness, d , of the unperturbed liquid layer. First of all, we will search for different unstable modes that dominate the primary instability in the low to high Reynolds number regime. Numerically, we have observed the existence of five distinct modes, which are called the H-mode (surface mode), surfactant mode, S-mode, P-mode, and shear mode. In general, H-mode, surfactant mode, S-mode, and P-mode trigger the primary instability in the low to moderate Reynolds number regime, while the shear mode triggers the primary instability in the high Reynolds number regime [12–14,57]. However, the H-mode and the shear mode compete with each other to control the primary instability in the high Reynolds number regime, depending on the magnitude of the inclination angle [12,14,49]. We have illustrated these distinct unstable modes in Fig. 5 for various sets of flow parameters. In fact, we have identified these distinct modes by their phase speeds because the phase speeds of these distinct modes are completely different from each other. To confirm our argument, we have further produced the numerical results corresponding to surface and surfactant modes in Figs. 5(e) and 5(f), respectively. We can see that the phase speed corresponding to the surface mode/H-mode is approximately equal to $c_{rs} \approx 2.0094$ when $k = 0.01$ and $\tau = 0.01$, which agrees well with the analytical result $c_{rs} \approx c_{0s} + k^2 c_{2s} = 2.00938$ because k lies in the long-wave region. Similarly, the phase speed corresponding to the surfactant mode is approximately equal to $c_{rm} \approx 1.4999$ when $k = 0.01$ and $\tau = 0.5$, which also agrees well with the analytical result $c_{rm} \approx c_{0m} + k^2 c_{2m} = 1.49997$ because k lies in the long-wave region. Indeed, we

TABLE II. Comparison between the analytical and numerical values of the critical surfactant Péclet number Pe_{cm} for the surfactant mode when the surfactant Marangoni number Ma_S varies. The other parameter values are $Ca = 2$, $\theta = 15^\circ$, $Pr = 7$, $Bi = 1$, $Ma_T = 25$, $Pe_T = 70$, $Re = 10$, and $\tau = 0.5$.

| Ma_S | Analytical value (Pe_{cm}) | Numerical value (Pe_{cm}) |
|--------|--------------------------------|-------------------------------|
| 1.0 | 4.0000 | 4.0025 |
| 2.0 | 2.0000 | 2.0019 |
| 3.0 | 1.3333 | 1.3336 |
| 4.0 | 1.0000 | 1.0008 |
| 5.0 | 0.8000 | 0.7994 |

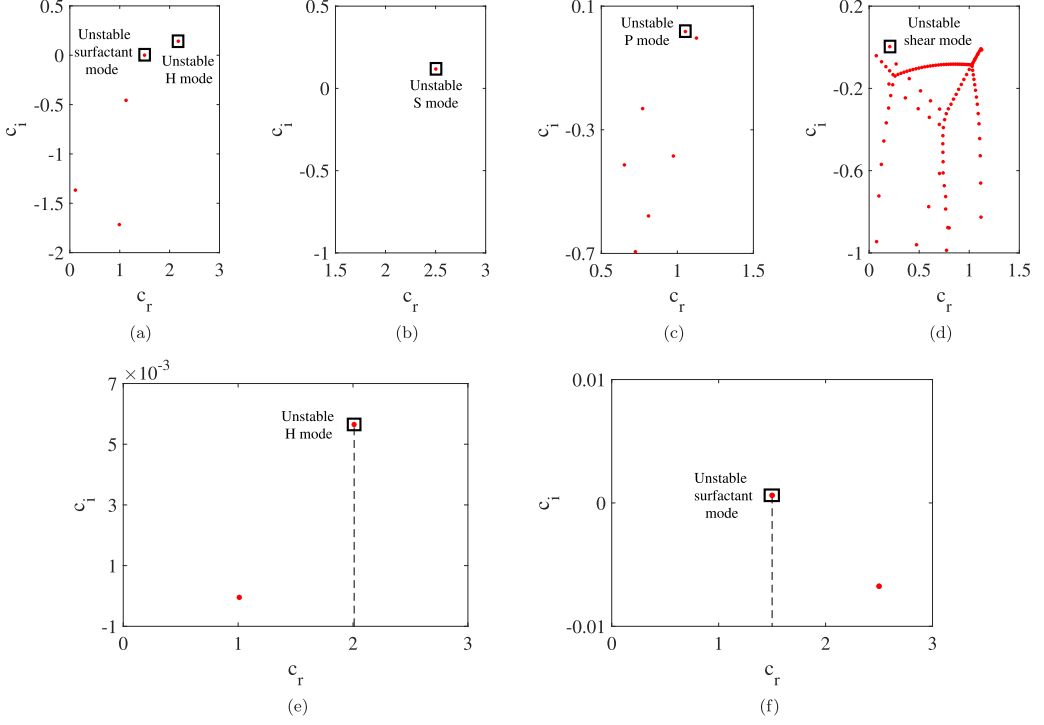


FIG. 5. Eigenvalues in (c_r, c_i) plane. (a) $\text{Re} = 11$, $\theta = 15^\circ$, $k = 0.2$, $M_T = 22$, $\text{Ka} = 500$, $M_S = 0.2$, $\text{Pe}_S = 160$, $B = 1$, and $\tau = 0.5$. (b) $\text{Re} = 0.22$, $\theta = 15^\circ$, $k = 0.05$, $M_T = 25$, $\text{Ka} = 500$, $M_S = 0.001$, $\text{Pe}_S = 1000$, $B = 1$, and $\tau = 0.5$. (c) $\text{Re} = 20$, $\theta = 15^\circ$, $k = 3$, $M_T = 55$, $\text{Ka} = 500$, $M_S = 0.02$, $\text{Pe}_S = 1000$, $B = 1$, and $\tau = 0.125$. (d) $\text{Re} = 8000$, $\theta = (1/60)^\circ$, $k = 1.8$, $M_T = 15$, $\text{Ka} = 51000$, $M_S = 0.001$, $\text{Pe}_S = 140$, $B = 1$, and $\tau = 0.05$. (e) $\text{Re} = 3$, $\theta = 15^\circ$, $k = 0.01$, $M_T = 5.15$, $\text{Ka} = 1.65$, $M_S = 3.3$, $\text{Pe}_S = 140$, $B = 0.55$, and $\tau = 0.01$. (f) $\text{Re} = 3$, $\theta = 15^\circ$, $k = 0.01$, $M_T = 3.3$, $\text{Ka} = 1.65$, $M_S = 1.65$, $\text{Pe}_S = 1000$, $B = 0.55$, and $\tau = 0.5$. The other parameter value is $\text{Pr} = 7$.

have chosen a small value of k in the numerical simulation to compare with the analytical results. The existence of more than one temporal mode, or equivalently, more than one value of ω , can also be figured out from the dispersion relation associated with the perturbation equations (28)–(37). In particular, a perturbation field $\psi'_p(x, t)$ in real space is connected to the Fourier variables k and ω in Fourier space by the following double Fourier integral [58,59]

$$\psi'_p(x, t) = \frac{1}{(2\pi)^2} \int_{L_\omega} \int_{F_k} \psi_p(k, \omega) \exp[i(kx - \omega t)] dk d\omega, \quad (91)$$

where L_ω and F_k are contours in the complex ω and k planes. Using Eq. (91), one can obtain an implicit dispersion relation involving angular frequency ω and wave number k corresponding to the perturbation equations (28)–(37). As unsteady terms are present in the perturbation momentum equations, perturbation energy equation, perturbation surfactant transport equation, and perturbation kinematic boundary condition, one can expect multiple values of ω from the dispersion relation.

A. Effects of the modified surfactant Marangoni number and the modified thermal Marangoni number on the H-mode, S-mode, and P-mode in the low to moderate Reynolds number regime

In this subsection we will decipher the effects of the surfactant Marangoni number and the thermal Marangoni number on the H-mode (surface mode), S-mode, and P-mode. To do that, we

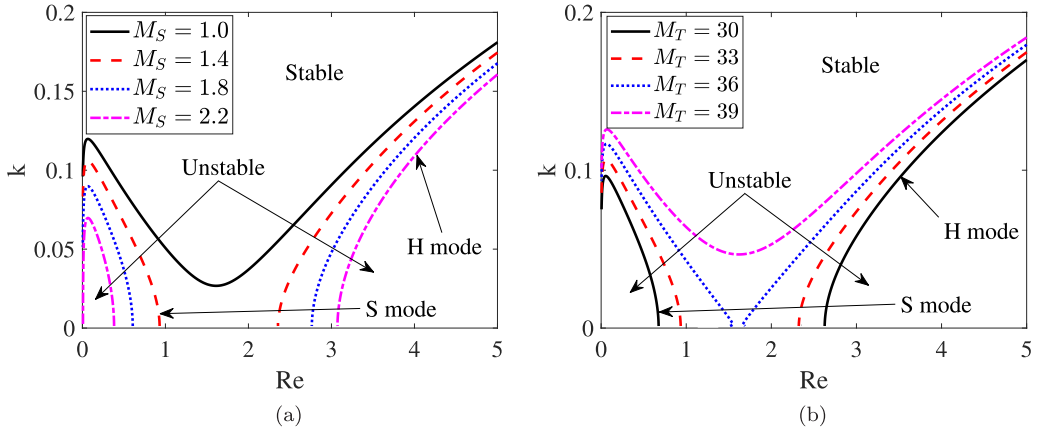


FIG. 6. (a) Variation of the neutral stability curves for the H-mode (surface mode) and S-mode in (Re, k) plane for different values of M_S when $M_T = 37$ and $\tau = 0.5$. (b) Variation of the neutral stability curves for the H-mode and S-mode in (Re, k) plane for different values of M_T when $M_S = 1$ and $\tau = 0.1$. The other parameter values are $Ka = 500$, $\theta = 15^\circ$, $Pr = 7$, $B = 1$, and $Pe_S = 1000$.

solve the Orr-Sommerfeld-type boundary value problem (40)–(47) numerically and compute the neutral stability curves for the H-mode and S-mode, respectively. In the numerical simulation, we vary the Reynolds number up to a moderate value. The ensuing results are depicted in Figs. 6(a) and 6(b), respectively. In Fig. 6(a) we see that there is only one neutral stability curve that separates the stable and unstable regions when $M_S = 1$, while the other flow parameters are fixed. This neutral stability curve is specified by a solid line in (Re, k) plane. However, if the value of M_S , or equivalently, the surfactant Marangoni number is increased, the neutral stability curve suddenly gets separated into two neutral stability curves. One curve is associated with the S-mode, while the other one is associated with the H-mode. In particular, the unstable zone generated by the S-mode neutral stability curve emerges in the low Reynolds number regime, while the unstable zone generated by the H-mode neutral stability curve emerges in the moderate Reynolds number regime. Clearly, if the value of M_S is further increased, the unstable zone induced by the S-mode gradually attenuates and finally disappears from the (Re, k) plane at higher values of M_S . Moreover, we see that the unstable zone induced by the H-mode also reduces as long as the modified surfactant Marangoni number increases. This fact indicates that the modified surfactant Marangoni number has a stabilizing effect on the S-mode and H-mode. In Fig. 6(b) we have again displayed the neutral stability curves for the H-mode and S-mode. However, in this case, the modified thermal Marangoni number is changed while the other flow parameters are constant. It should be noted that there are two separate unstable zones when $M_T = 30$. Hence, there are two neutral stability curves; one curve is pertaining to the S-mode, while the other curve is pertaining to the H-mode. These neutral stability curves are specified by solid lines. Interestingly, these unstable zones created by the neutral stability curves magnify as long as the modified thermal Marangoni number increases, and ultimately, they merge together and form one unstable region. This fact indicates the destabilizing role of the modified thermal Marangoni number in the S-mode and H-mode, which is in contrast to the stabilizing role of the modified surfactant Marangoni number in the S-mode and H-mode. Next, we have computed the neutral stability curve for the thermocapillary P-mode when only the modified surfactant Marangoni number changes. The associated result is depicted in Fig. 7(a). Obviously, the neutral stability curve for the P-mode has an island shape. It is interesting to note that the P-mode unstable zone emerges in the finite wave number zone rather than the long-wave zone. Unlike the S-mode instability, we observe that the unstable zone created due to the P-mode instability decreases as long as the modified surfactant Marangoni number increases and ultimately disappears

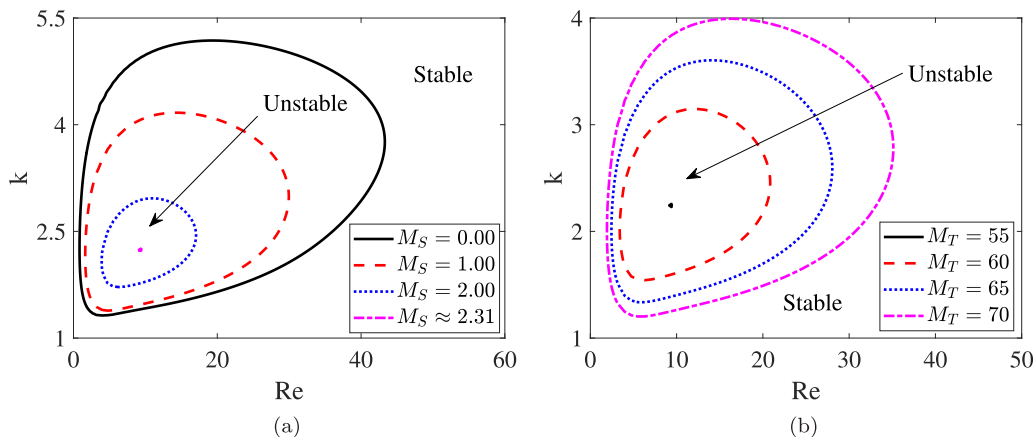


FIG. 7. (a) Variation of the neutral stability curve for the P-mode in (Re, k) plane for different values of M_S when $M_T = 55$. (b) Variation of the neutral stability curve for the P-mode in (Re, k) plane for different values of M_T when $M_S \approx 2.31$. The other parameter values are $\text{Ka} = 500$, $\theta = 15^\circ$, $\text{Pr} = 7$, $B = 1$, $\tau = 0.125$, and $\text{Pe}_S = 1000$.

from the neutral diagram at higher values of the modified surfactant Marangoni number. Hence, the modified surfactant Marangoni number also stabilizes the thermocapillary P-mode instability. On the other hand, if the modified thermal Marangoni number is varied, we observe an opposite phenomenon, i.e., the unstable zone created by the P-mode instability magnifies as the modified thermal Marangoni number increases [see Fig. 7(b)]. Therefore, the modified thermal Marangoni number destabilizes the P-mode instability. Physically, with the increasing value of the modified surfactant Marangoni number, the surface tension gradient increases, or equivalently, the local flow induced by the surfactant Marangoni traction from the crest-to-trough direction of the deformed liquid film surface increases and yields a stabilizing influence. Instead of varying the modified surfactant Marangoni number, if the modified thermal Marangoni number is increased, the surface tension of the liquid film decreases, which leads to a destabilizing effect.

B. Effects of the modified thermal Marangoni number, modified surfactant Marangoni number, and modified Biot number on the surfactant mode

Now we will explore the individual effects of different flow parameters on the surfactant mode. To do that, the Orr-Sommerfeld-type boundary value problem (40)–(47) is solved numerically, and the neutral stability curve and temporal growth rate for the surfactant mode are computed. Figure 8(a) demonstrates the variation of the neutral stability curve for the surfactant mode when the modified thermal Marangoni number and the modified surfactant Marangoni number are altered but other flow parameters are kept constant. Initially, we fix the modified surfactant Marangoni number in the numerical simulation. Clearly, we notice that the unstable zone created by the neutral stability curve magnifies as the modified thermal Marangoni number increases. However, the onset of primary instability for the surfactant mode does not vary with the change in the modified thermal Marangoni number because the critical surfactant Péclet number, above which the surfactant mode instability emerges, is independent of the thermal Marangoni number Ma_T [see also Eq. (80)]. This result indicates the destabilizing impact of the modified thermal Marangoni number on the surfactant mode. However, if the modified surfactant Marangoni number is varied, the onset of surfactant mode instability shifts towards the left, i.e., the critical surfactant Péclet number decreases with increasing M_S . Moreover, the unstable zone generated by the neutral stability curve is enhanced in the presence of the modified surfactant Marangoni number. Hence, unlike the modified thermal Marangoni number, the modified surfactant Marangoni number also destabilizes the surfactant mode

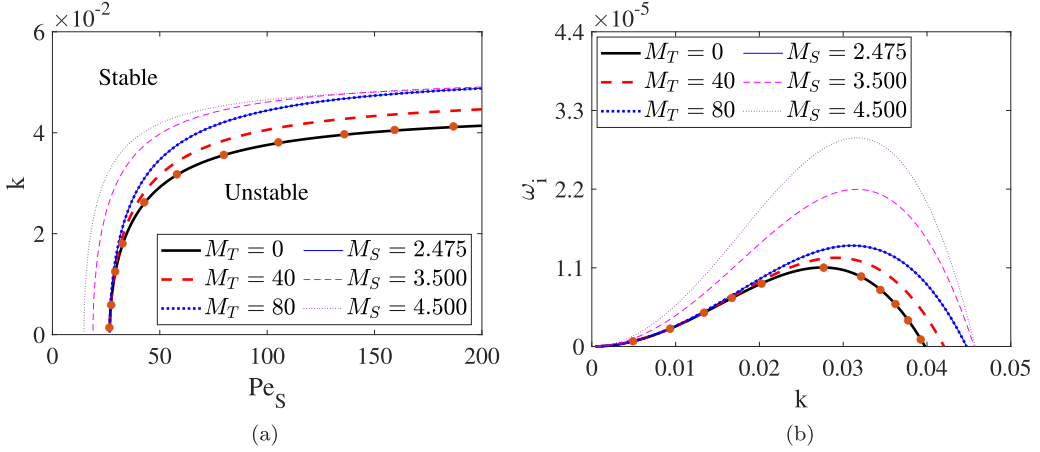


FIG. 8. (a) Variation of the neutral stability curve for the surfactant mode in (Pe_S, k) plane for different values of M_T when $M_S = 2.475$ as well as for different values of M_S when $M_T = 80$. (b) Variation of the temporal growth rate ω_i for the surfactant mode with streamwise wave number k for different values of M_T when $Pe_S = 140$ and $M_S = 2.475$ as well as for different values of M_S when $Pe_S = 140$ and $M_T = 80$. The other parameter values are $Re = 3$, $\theta = 4^\circ$, $Ca = 2$, $Pr = 7$, $B = 1$, and $\tau = 0.1$. The solid points are the results of Bhat and Samanta [36].

instability. To strengthen our above findings, we have further demonstrated the numerical result pertaining to the temporal growth rate of the surfactant mode for a fixed value of the surfactant Péclet number Pe_S selected from the unstable zone. Again, one can see that the temporal growth rate for the surfactant mode intensifies as the modified thermal Marangoni number and the modified surfactant Marangoni number increase [see Fig. 8(b)]. These results fully support the destabilizing influences of both the modified thermal Marangoni number and the modified surfactant Marangoni number on the surfactant mode. Physically, with an increase in the value of the modified thermal Marangoni number, the surface tension decreases as the temperature of the viscous film rises. This fact prevents the local flow from occurring in the crest-to-trough direction due to the surfactant Marangoni traction, which leads to a destabilizing effect on the surfactant mode. Next, we have shown the individual effect of the modified Biot number on the surfactant mode. Here we perceive that the modified Biot number exhibits a dual role in the surfactant mode instability. To disclose these peculiar results, we have first computed the neutral stability curve and temporal growth rate for the surfactant mode when the modified Biot number changes, but it takes a value smaller than or equal to 0.5 ($B \leq 0.5$) when $Re = 3$, $\theta = 4^\circ$, $Ca = 2$, $Pr = 7$, $M_T = 80$, $M_S = 2.475$, and $\tau = 0.1$. Figure 9(a) reveals the variation of the neutral stability curve in (Pe_S, k) plane. In this case, the unstable zone bounded by the neutral stability curve enhances as the modified Biot number increases. This result indicates the destabilizing influence of the modified Biot number on the surfactant mode. Again, we have observed that the critical surfactant Péclet number for the onset of primary instability for the surfactant mode remains the same for the various values of the modified Biot number because it is not a function of the modified Biot number [see also Eq. (80)]. To support the above numerical result, the temporal growth rate is also depicted with an increase in the value of the modified Biot number, where the temporal growth rate becomes stronger in the presence of the modified Biot number [see Fig. 9(b)]. This event is consistent with the destabilizing role of the modified Biot number in the surfactant mode. Second, we have produced the results when the modified Biot number takes a value greater than or equal to 0.5 ($B \geq 0.5$) when $Re = 3$, $\theta = 4^\circ$, $Ca = 2$, $Pr = 7$, $M_T = 80$, $M_S = 2.475$, and $\tau = 0.1$. Figure 9(c) displays the variation of the neutral stability curve with the modified Biot number. Clearly, the unstable zone attenuates as the modified Biot number increases. To ensure this result, we have also plotted the temporal growth

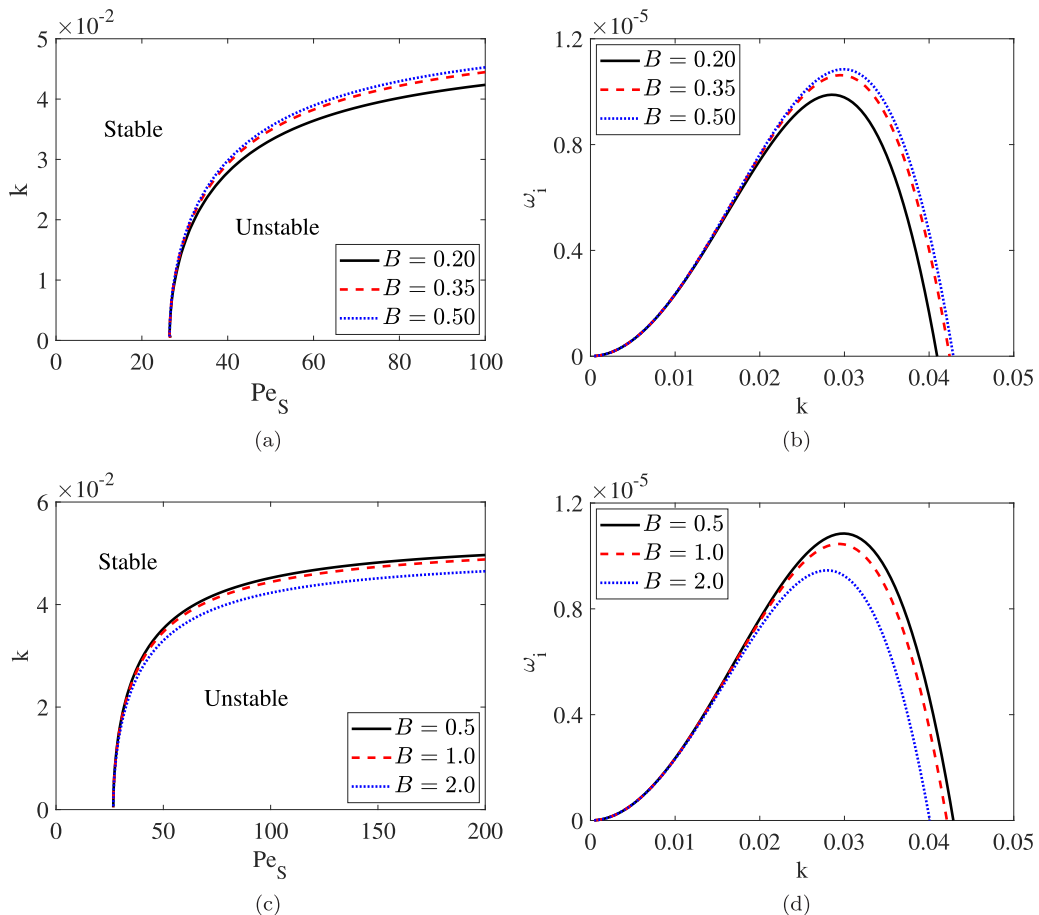


FIG. 9. (a) Variation of the neutral stability curve for the surfactant mode in (Pe_S, k) plane for different values of B ($B \leq 0.5$). (b) Variation of the temporal growth rate ω_i for the surfactant mode for different values of B when $Pe_S = 80$. (c) Variation of the neutral stability curve for the surfactant mode in (Pe_S, k) plane for different values of B ($B \geq 0.5$). (d) Variation of the temporal growth rate ω_i for the surfactant mode for different values of B when $Pe_S = 80$. The other parameter values are $Re = 3$, $\theta = 4^\circ$, $Ca = 2$, $Pr = 7$, $M_T = 80$, $M_S = 2.475$, and $\tau = 0.1$.

rate [see Fig. 9(d)]. Here one can see that the temporal growth rate becomes weaker as the modified Biot number increases, which indicates a stabilizing influence of the modified Biot number on the surfactant mode.

C. Effects of the surfactant Marangoni number and thermal Marangoni number on the shear mode

In this subsection, we will explore the shear mode, which generally emerges in the high Reynolds number regime when the inclination angle is very low [11–14,57]. This mode is retrieved by its phase speed as the shear mode has a smaller phase speed than the surface mode [32] [see also Fig. 5]. The neutral stability curve for the shear mode is computed numerically and demonstrated in Fig. 10(a) when the surfactant Marangoni number increases while the other flow parameters are kept at constant values. We can see that the unstable zone created by the neutral stability curve decreases gradually as long as the surfactant Marangoni number increases, which is followed by the successive promotion of the critical Reynolds number for the onset of shear mode instability. This result implies

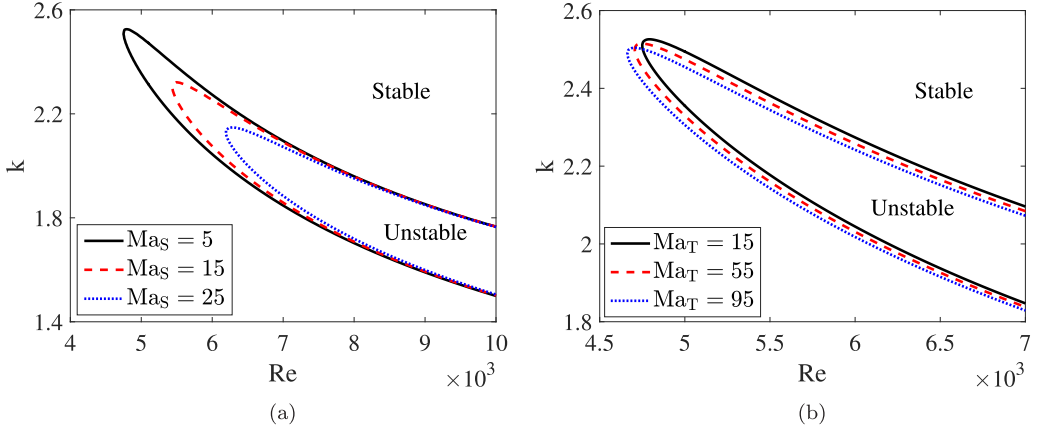


FIG. 10. (a) Variation of the neutral stability curve for the shear mode in (Re, k) plane for different values of the surfactant Marangoni number Ma_S when $Ma_T = 15$. (b) Variation of the neutral stability curve for the shear mode in (Re, k) plane for different values of the thermal Marangoni number Ma_T when $Ma_S = 5$. The other parameter values are $Bi = 1$, $Pr = 7$, $Pe_S = 1000$, $\theta = (1^\circ/60)$, $Ca = 2$, and $\tau = 0.1$.

that the surfactant Marangoni number has a stabilizing effect on the shear mode, as shown in the case of the surface mode. As before, however, if the thermal Marangoni number is increased, the critical Reynolds number for the onset of the shear mode instability is decreased, which is fully opposite to the role of the surfactant Marangoni number in the shear mode [see Fig. 10(b)]. How the critical Reynolds number for the shear mode instability alters with the surfactant Marangoni number and the thermal Marangoni number is shown in Fig. 11(a). The results reveal that the increment of the threshold of instability for the shear mode with increasing Ma_S happens at a faster rate than

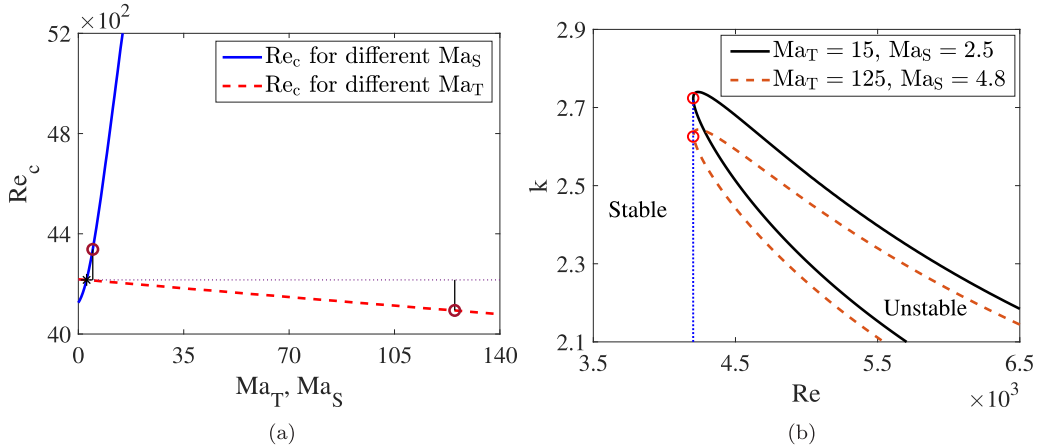


FIG. 11. (a) Variation of the critical Reynolds number Re_c for the shear mode instability when the surfactant Marangoni number Ma_S and the thermal Marangoni number Ma_T vary. Solid line stands for the variation of Re_c with Ma_S when $Ma_T = 15$ and dashed line stands for the variation of Re_c with Ma_T when $Ma_S = 2.5$. Star point represents data ($Ma_S = 2.5$, $Ma_T = 15$). The circular symbols in solid and dashed lines represent the data $Ma_S = 4.8$ and $Ma_T = 125$, respectively. (b) Variation of the neutral stability curve for the shear mode in (Re, k) plane. Solid line represents the result for $Ma_S = 2.5$ and $Ma_T = 15$. Dashed line represents the result for $Ma_S = 4.7$ and $Ma_T = 125$. The other parameter values are $Bi = 1$, $Pr = 7$, $Pe_S = 1000$, $\theta = (1^\circ/60)$, $Ca = 2$, and $\tau = 0.1$.

its decrement with increasing Ma_T . However, we can equalize these variations by using a larger change of Ma_T and a smaller change of Ma_S so that the critical Reynolds number for the shear mode instability will be the same. In other words, we can neutralize the increment of Re_c due to the increase of Ma_S and the decrement of Re_c due to the increase of Ma_T . To strengthen our claim, we first choose the crossing point ($\text{Ma}_S = 2.5$, $\text{Ma}_T = 15$) and draw the neutral stability curve in Fig. 11(b). Next, we select the point ($\text{Ma}_S = 4.8$, $\text{Ma}_T = 125$) in such a way that the increment and decrement of Re_c are the same. Again, we draw the neutral stability curve in Fig. 11(b) when $\text{Ma}_S = 4.8$, $\text{Ma}_T = 125$. Indeed, the critical Reynolds number, or equivalently, the threshold of instability for the shear mode, is the same in both cases.

V. INERTIALESS STABILITY ANALYSIS

This section concerns the linear stability of surfactant-laden nonisothermal film flow in the inertialess limit, i.e., when $\text{Re} \rightarrow 0$. As a consequence, the Orr-Sommerfeld-type boundary value problem (40)–(47) simplifies into the following forms:

$$(D^2 - k^2)^2 \hat{\phi} = 0, \quad 0 \leq y \leq 1, \quad (92)$$

$$(D^2 - k^2) \hat{T} = 0, \quad 0 \leq y \leq 1, \quad (93)$$

$$\hat{\phi} = 0, \quad \hat{T} = 0, \quad D\hat{\phi} = 0, \quad \text{at } y = 0, \quad (94)$$

$$(D^2 + k^2) \hat{\phi} + ik\text{Ma}_T(\hat{T} + D\bar{T}\hat{\eta}) + ik\text{Ma}_S\hat{\Gamma} + D^2\bar{U}\hat{\eta} = 0, \quad \text{at } y = 1, \quad (95)$$

$$D^3\hat{\phi} - 3k^2D\hat{\phi} = ik\hat{\eta}[k^2(\text{Ca}^{-1} - \text{Ma}_T\bar{T}) - D\bar{P} - 2ikD\bar{U}], \quad \text{at } y = 1, \quad (96)$$

$$D\hat{T} + \text{Bi}[\hat{T} + D\bar{T}\hat{\eta}] = 0, \quad \text{at } y = 1, \quad (97)$$

$$D\hat{\phi} + \left[(\bar{U} - c) - \frac{ik}{\text{Pe}_s} \right] \hat{\Gamma} + D\bar{U}\hat{\eta} = 0, \quad \text{at } y = 1, \quad (98)$$

$$\hat{\phi} + (\bar{U} - c)\hat{\eta} = 0, \quad \text{at } y = 1. \quad (99)$$

We solve the above boundary value problems (92)–(99) analytically and express the general solution in the following form:

$$\hat{\phi}(y) = p_1 e^{ky} + p_2 e^{-ky} + p_3 y e^{ky} + p_4 y e^{-ky}, \quad (100)$$

$$\hat{T}(y) = p_5 e^{ky} + p_6 e^{-ky}. \quad (101)$$

Here p_1 , p_2 , p_3 , p_4 , p_5 , and p_6 denote the integration constants. Using the boundary conditions (94)–(99), we can obtain a set of algebraic equations in terms of the unknown variables p_1 , p_2 , p_3 , p_4 , p_5 , p_6 , $\hat{\Gamma}$, and $\hat{\eta}$. This set of equations is further cast into a homogeneous matrix equation form as follows:

$$\mathcal{N}\mathcal{X} = 0, \quad (102)$$

where

$$\mathcal{N} = \begin{pmatrix} 1 & 1 & 0 & 0 & 0 & 0 & 0 & 0 \\ k & -k & 1 & 1 & 0 & 0 & 0 & 0 \\ 0 & 0 & 0 & 0 & 1 & 1 & 0 & 0 \\ 2k^2 e^k & 2k^2 e^{-k} & 2k(k+1)e^k & 2k(k-1)e^{-k} & k^2 \text{Ma}_T e^k & k^2 \text{Ma}_T e^{-k} & ik \text{Ma}_S & -(2 + \frac{ik \text{Ma}_T \text{Bi}}{1+\text{Bi}}) \\ -2k^3 e^k & 2k^3 e^{-k} & -2k^3 e^k & 2k^3 e^{-k} & 0 & 0 & 0 & -ik[k^2(\text{Ca}^{-1} - \frac{\text{Ma}_T}{1+\text{Bi}}) - D\bar{P} - 2ik\tau] \\ 0 & 0 & 0 & 0 & (\text{Bi} + k)e^k & (\text{Bi} - k)e^{-k} & 0 & -\frac{\text{Bi}^2}{1+\text{Bi}} \\ ke^k & -ke^{-k} & (1+k)e^k & (1-k)e^{-k} & 0 & 0 & \bar{U} - c - \frac{ik}{\text{Pe}_S} & -2 \\ e^k & e^{-k} & e^k & e^{-k} & 0 & 0 & 0 & (1 + \tau) - c \end{pmatrix}$$

and

$$\mathcal{X} = \begin{pmatrix} p_1 \\ p_2 \\ p_3 \\ p_4 \\ p_5 \\ p_6 \\ \hat{\Gamma} \\ \hat{\eta} \end{pmatrix}.$$

Hence, for a nontrivial solution of the homogeneous system (102), the determinant of the matrix \mathcal{N} has to be zero. Therefore, one can have

$$\det(\mathcal{N}) = 0, \quad (103)$$

which finally provides the following dispersion relation for the nonisothermal surfactant-laden inertialess film flow

$$\mathcal{F}(c, k, \text{Ma}_T, \text{Ma}_S, \text{Pe}_S, \text{Ca}, \text{Bi}, \tau, \theta) = 0. \quad (104)$$

Note that the dispersion relation (104) is a quadratic function of c , and therefore, it will supply two distinct roots of c : one root corresponds to the H-mode (surface mode), and the other root corresponds to the surfactant mode. Now we use the long-wave analysis ($k \rightarrow 0$) to determine the complex wave speeds for the H-mode and the surfactant mode, respectively. The analytical expressions are the following:

$$\begin{aligned} c_s &= (2 + \tau) - \frac{i}{6} \left[4 \cot \theta - \frac{3\text{Ma}_T \text{Bi}}{(1 + \text{Bi})^2} + 3\text{Ma}_S(2 + \tau) \right] k \\ &\quad - \frac{1}{12} \left\{ \text{Ma}_S \left[2 \cot \theta - \frac{6(2 + \tau)}{\text{Pe}_S} + \tau \left(4 \cot \theta - \frac{3\text{Bi} \text{Ma}_T}{(1 + \text{Bi})^2} 3\text{Ma}_S(2 + \tau) \right) \right] - 8(3 + \tau) \right\} k^2 \\ &\quad + \frac{i}{360(1 + \text{Bi})^4 \text{Pe}_S^2} (m_0 + m_1 \text{Pe}_S + m_2 \text{Pe}_S^2 + m_3 \text{Ma}_T + m_4 \text{Ma}_T^2) k^3 + O(k^4), \end{aligned} \quad (105)$$

$$\begin{aligned} c_m &= (1 + \tau) + \frac{i}{2} \left(\text{Ma}_S \tau - \frac{2}{\text{Pe}_S} \right) k \\ &\quad - \frac{\text{Ma}_S}{12} \left\{ -2 \cot \theta + \frac{6(2 + \tau)}{\text{Pe}_S} + \tau \left[\frac{3\text{Bi} \text{Ma}_T}{(1 + \text{Bi})^2} - 4 \cot \theta - 3\text{Ma}_S(2 + \tau) \right] \right\} k^2 \\ &\quad + \frac{i \text{Ma}_S}{72(1 + \text{Bi})^4 \text{Pe}_S^2} (n_0 + n_1 \text{Pe}_S + n_2 \text{Pe}_S^2 + n_3 \text{Ma}_T + n_4 \text{Ma}_T^2) k^3 + O(k^4), \end{aligned} \quad (106)$$

where

$$\begin{aligned}
 m_0 &= 180(1 + \text{Bi})^4 \text{Ma}_S(2 + \tau), \\
 m_1 &= -30(1 + \text{Bi})^4 \text{Ma}_S[-3\text{Ma}_S(2 + \tau)(2 + 3\tau) + 2 \cot \theta(5 + 4\tau)], \\
 m_2 &= 2(1 + \text{Bi})^4(216 \cot \theta - 60\text{Ca}^{-1} + 5\text{Ma}_S\{4(14 + \csc^2 \theta) + 2(4 \csc^2 \theta - 6\tau - 7)\tau \\
 &\quad + 9\text{Ma}_S^2 \tau(1 + \tau)(2 + \tau) + 6 \cot \theta \text{Ma}_S[1 + \tau(5 + 3\tau)]\}), \\
 m_3 &= -15(1 + \text{Bi})\text{Pe}_S\{4[\text{Bi}(2 + 3\text{Bi}) - 2]\text{Pe}_S + 3\text{Bi}(1 + \text{Bi})\text{Ma}_S^2 \text{Pe}_S \tau(4 + 3\tau) \\
 &\quad + 2\text{Bi}(1 + \text{Bi})\text{Ma}_S[\text{Pe}_S(1 + 4\tau) \cot \theta - 6(1 + \tau)]\}, \\
 m_4 &= 45\text{Bi}^2 \text{Ma}_S \text{Pe}_S^2 \tau, \\
 n_0 &= 36(1 + \text{Bi})^4(2 + \tau), \\
 n_1 &= -6(1 + \text{Bi})^4[3\text{Ma}_S(2 + \tau)(2 + 3\tau) + 2 \cot \theta(5 + 4\tau)], \\
 n_2 &= 2(1 + \text{Bi})^4\{9\text{Ma}_S^2 \tau(1 + \tau)(2 + \tau) + 2(2 \cot^2 \theta - 3\tau)(1 + 2\tau) \\
 &\quad + 6 \cot \theta \text{Ma}_S[1 + \tau(5 + 3\tau)]\}, \\
 n_3 &= 3\text{Bi} \text{Pe}_S(1 + \text{Bi})^2(12(1 + \tau) - \text{Pe}_S\{2 \cot \theta + \tau[8 \cot \theta + 3\text{Ma}_S(4 + 3\tau)]\}), \\
 n_4 &= 9\text{Bi}^2 \text{Pe}_S^2 \tau.
 \end{aligned}$$

The next step is to use the neutral stability condition, $c_i \approx |kc_{1s}| = 0$, in the limit $k \rightarrow 0$, which leads to the analytical expression of the onset of H-mode instability in the inertialess approximation

$$\frac{\text{Ma}_S}{\text{Ma}_T} = \frac{\text{Bi}}{(1 + \text{Bi})^2(2 + \tau)} - \frac{4}{3} \frac{\cot \theta}{(2 + \tau)\text{Ma}_T}. \quad (107)$$

Equation (107) coincides with the expression (73) when the Reynolds number is set to zero. Furthermore, if $\theta = \pi/2$, and $\frac{\text{Ma}_S}{\text{Ma}_T} > \frac{\text{Bi}}{(1 + \text{Bi})^2(2 + \tau)}$, the infinitesimal disturbance will be completely stable. In other words, if the stabilizing surfactant effect dominates the destabilizing thermal effect, the infinitesimal disturbance will be damped in the inertialess approximation. However, one can make this stable disturbance unstable by including inertia terms in the momentum equations [see also Eq. (75)]. In a similar fashion, we determine the onset of instability for the surfactant mode,

$$\text{Pe}_{\text{Sc}} = \frac{2}{\tau \text{Ma}_S}, \quad (108)$$

which is exactly the same as determined for the flow configuration when inertia is present. This result shows that the Reynolds number, or equivalently, inertia has no impact on the onset of surfactant mode instability. Figure 12(a) reveals the comparison between the results obtained numerically from the inertialess approximation (solid line), the long-wave third-order approximation (dashed line), the long-wave fifth-order approximation (dotted line), and the Padé approximation (dash-dotted line). Clearly, we can see that the Padé approximation result almost accurately captures the numerical result. However, the long-wave third-order result has a much larger deviation from the numerical result in comparison with the long-wave fifth-order result. Figures 12(b) and 12(c), respectively, display the neutral stability curve and temporal growth rate for the surfactant mode. More specifically, we have compared the results with inertia and without inertia when the thermal Marangoni number varies. Obviously, the Reynolds number has no influence on the threshold of instability for the surfactant mode. However, the unstable zone induced by the surfactant mode's neutral stability curve diminishes in the presence of inertia. This fact implies that inertia has a stabilizing effect on the surfactant mode. On the other hand, the surfactant mode instability becomes stronger as the thermal Marangoni number increases because the unstable zone magnifies with Ma_T . These results are further confirmed by the plot of the temporal growth rate [see Fig. 12(c)].

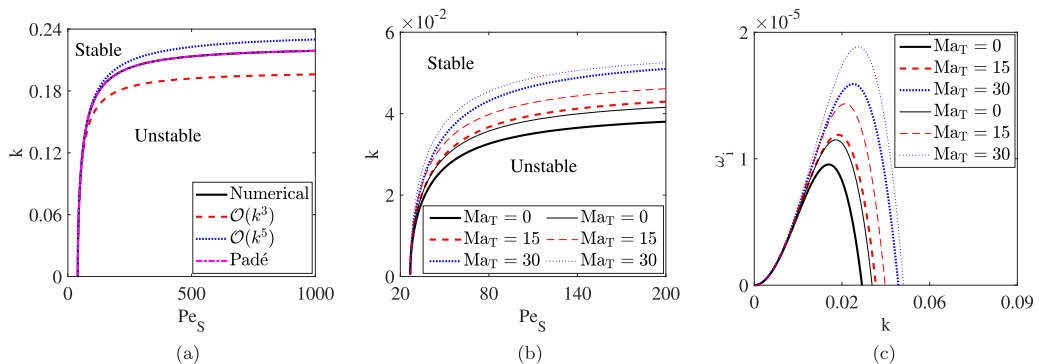


FIG. 12. (a) Variation of the neutral stability curve for the surfactant mode in (Pe_S, k) plane when $Re = 0$, $Ca = 2$, $Ma_S = 0.5$, $Bi = 1$, $Ma_T = 10$, $\theta = 15^\circ$, and $\tau = 0.1$. Solid, dashed, dotted, and dash-dotted lines stand for the numerical result, the long-wave third-order result, the long-wave fifth-order result, and the Padé approximation, respectively. (b) Variation of the neutral stability curve for the surfactant mode in (Pe_S, k) plane for different values of Ma_T . (c) Variation of the temporal growth rate ω_i with wave number k when Ma_T changes and $Pe_S = 150$. Thick lines represent the results with inertia ($Re = 80$) and thin lines represent the results without inertia ($Re = 0$). The other parameter values are $Ca = 2$, $Ma_S = 0.75$, $Bi = 1$, $Pe_T = 560$, $\theta = 4^\circ$, and $\tau = 0.1$.

VI. SUMMARY AND CONCLUSIONS

The linear thermocapillary instability is investigated for a two-dimensional gravity-driven shear-imposed incompressible viscous film flowing over a uniformly heated inclined wall. It is assumed that the film surface is contaminated by an insoluble surfactant. As the film flow is nonisothermal, we have also included the energy equation in the set of governing equations. To explore the different unstable modes, we have formulated the Orr-Sommerfeld-type equation. In particular, two different approaches are followed to solve the boundary value problem. The analytical approach is nothing but long-wave analysis, which shows the existence of H-mode (surface mode) and surfactant mode. The results reveal that the H-mode is stabilized by the surfactant Marangoni number but destabilized by the thermal Marangoni number. Therefore, one can retrieve an analytical relationship between the surfactant and thermal Marangoni numbers for which the critical Reynolds number for the H-mode instability will be completely independent of the nonisothermal effects.

Because of the convergence issue of the long-wave analysis, we have also computed the analytical result based on the Padé approximation. Clearly, the results acquired from the third-order and fifth-order long-wave analyses are less accurate than those obtained from the Padé approximation when the comparison is performed with the numerical results. On the other hand, the numerical results reveal the existence of five unstable modes, which can trigger the primary instability in the low to high Reynolds number regime. In particular, the H-mode (surface mode) emerges due to the streamwise component of gravitational force, the surfactant mode emerges due to the transport of insoluble surfactant at the liquid film surface, the S-mode and P-mode appear due to the thermocapillary effect, and the shear mode appears due to the viscous effect. These distinct unstable modes are recognized by their phase speeds, as they are different from each other.

Moreover, it is observed that the thermocapillary S-mode and P-mode instabilities are weakened in the presence of the insoluble surfactant at the liquid film surface. In fact, these thermocapillary primary instabilities can be completely suppressed by increasing the magnitude of the modified surfactant Marangoni number. However, if the modified thermal Marangoni number is increased in the numerical simulation, the S-mode and P-mode instabilities are intensified. More specifically, the impact of the modified thermal Marangoni number opposes the impact of the modified surfactant Marangoni number on the S-mode and P-mode instabilities.

TABLE III. Brief description of the physical effects of various dimensionless numbers on the different unstable modes.

| Unstable modes | Dimensionless numbers | Physical effect |
|-----------------|-----------------------|-----------------|
| H-mode | M_S | Stabilizing |
| | M_T | Destabilizing |
| S-mode | M_S | Stabilizing |
| | M_T | Destabilizing |
| P-mode | M_S | Stabilizing |
| | M_T | Destabilizing |
| Surfactant mode | M_S | Destabilizing |
| | M_T | Destabilizing |
| | $B(< 0.5)$ | Destabilizing |
| | $B(\geq 0.5)$ | Stabilizing |
| Shear mode | Ma_S | Stabilizing |
| | Ma_T | Destabilizing |

In the case of the surfactant mode, we notice that the unstable region induced by the neutral stability curve magnifies, and the associated temporal growth rate amplifies with the increase in the value of the modified thermal Marangoni number. Therefore, the surfactant mode instability is destabilized by the modified thermal Marangoni number. However, the critical surfactant Péclet number, above which the surfactant mode instability occurs, remains the same as it is independent of the modified thermal Marangoni number. In contrast, the critical surfactant Péclet number for the onset of the surfactant mode instability decreases as the modified surfactant Marangoni number increases because it is explicitly dependent on the surfactant Marangoni number. When we analyze the effect of the modified Biot number on the surfactant mode, it exhibits a peculiar behavior. We perceive that an increase in the modified Biot number enhances the surfactant mode instability when it keeps a value lower than or equal to 0.5 ($B \leq 0.5$). As soon as it keeps a value higher than or equal to 0.5 ($B \geq 0.5$), the result becomes fully opposite. That is, for values of B higher than or equal to 0.5, increasing the modified Biot number instead stabilizes the surfactant mode instability.

If the Reynolds number is kept at a high value but the inclination angle is kept at a low value, another mode arises, which is called the shear mode. The numerical results show that the instability induced by the shear mode attenuates with increasing values of the surfactant Marangoni number. Furthermore, the critical Reynolds number for the onset of the shear mode instability increases as the surfactant Marangoni number increases. However, the increment of the critical Reynolds number for the shear mode can be reduced by increasing the value of the thermal Marangoni number because the onset of the shear mode instability decreases in the presence of the thermal Marangoni number. In fact, for a given value of the surfactant Marangoni number, we can find a value of the thermal Marangoni number for which the threshold of instability for the shear mode will remain the same. The key results of the current study are further briefly presented in Table III.

Finally, the instability analysis is carried out in the inertialess approximation. In this case, we have found the H-mode and the surfactant mode. The long-wave analysis reveals that the infinitesimal disturbance becomes stable when the stabilizing surfactant effect dominates the destabilizing thermal effect ($\frac{Ma_S}{Ma_T} > \frac{Bi}{(1+Bi)^2(2+\tau)}$). However, this stable disturbance can be made unstable by adding inertia to the momentum equations. Moreover, we see that the Reynolds number, or equivalently, inertia has no role in the onset of the surfactant mode instability. But the unstable zone for the surfactant mode in the finite wave number regime is suppressed in the presence of inertia, which yields a stabilizing impact on the surfactant mode.

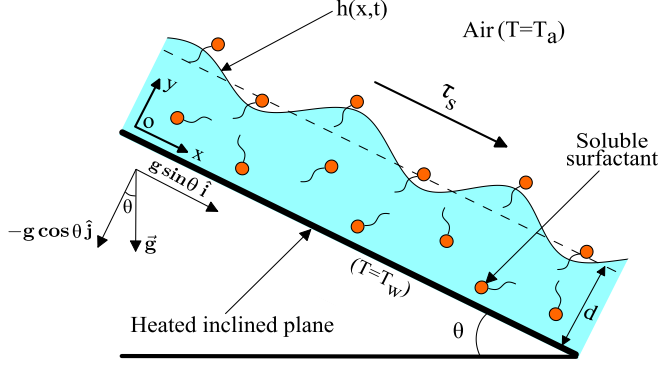


FIG. 13. Schematic diagram of a thin viscous liquid film with a soluble surfactant flowing down a uniformly heated inclined plane in the presence of a constant shear stress τ_s acting in the co-flow direction. Here d is the height of the unperturbed film flow, and $h(x, t)$ is the height of the perturbed film flow.

ACKNOWLEDGMENT

We would like to thank the anonymous referees for their comments and suggestions on improving the manuscript.

APPENDIX: THERMOCAPILLARY INSTABILITY OF A SHEAR-IMPOSED FILM FLOW WITH SOLUBLE SURFACTANT

In this Appendix we discuss the thermocapillary instability of a gravity-driven film flow contaminated by a soluble surfactant. In particular, the liquid flows down a uniformly heated inclined plane, where the temperature at the plane, $T = T_w$, is greater than the constant ambient temperature of $T = T_a$. The flow configuration is exactly similar to that of D'Alessio *et al.* [27]. However, a constant shear stress $\tau_s (> 0)$ is imposed at the liquid film surface in the co-flow direction. In Fig. 13 we have illustrated the schematic of the flow problem under consideration. To describe the nonisothermal liquid film flow, we have employed the following mass conservation, momentum, and energy equations:

$$\partial_x u + \partial_y v = 0, \quad (\text{A1})$$

$$\rho(\partial_t u + u\partial_x u + v\partial_y u) = -\partial_x p + \mu(\partial_{xx} u + \partial_{yy} u) + \rho g \sin \theta, \quad (\text{A2})$$

$$\rho(\partial_t v + u\partial_x v + v\partial_y v) = -\partial_y p + \mu(\partial_{xx} v + \partial_{yy} v) - \rho g \cos \theta, \quad (\text{A3})$$

$$\rho c_p(\partial_t T + u\partial_x T + v\partial_y T) = \kappa(\partial_{xx} T + \partial_{yy} T). \quad (\text{A4})$$

As we are interested in examining the effect of soluble surfactant on the thermocapillary instability, we will take two different concentrations: one pertains to the surfactant absorbed at the liquid film surface, while other pertains to the surfactant dissolved in the bulk. Moreover, we assume that the surfactants are existed in the liquid as monomers and they do not form micelles. Hence, the mass conservation of soluble surfactant in the bulk is governed by the following advection-diffusion equation [27,60,61]:

$$(\partial_t c_b + u\partial_x c_b + v\partial_y c_b) = D_b(\partial_{xx} c_b + \partial_{yy} c_b), \quad (\text{A5})$$

where c_b is the concentration of the soluble surfactant dissolved in the bulk and D_b is the surfactant diffusivity in the bulk. On the other hand, the transport of surfactant absorbed at the liquid film

surface, $y = h(x, t)$, is described by the following equation [27,62,63]:

$$\begin{aligned} \partial_t \Gamma + u \partial_x \Gamma + \frac{\Gamma}{1 + (\partial_x h)^2} [\partial_x u + \partial_x h \partial_x v + \partial_x h (\partial_y u + \partial_x h \partial_y v)] \\ = \frac{D_s}{\sqrt{1 + (\partial_x h)^2}} \partial_x [\partial_x \Gamma / \sqrt{1 + (\partial_x h)^2}] + J_{ba}, \end{aligned} \quad (\text{A6})$$

where $\Gamma(x, t)$ is the concentration of the surfactant absorbed at the liquid film surface, D_s is the surface surfactant diffusivity, and J_{ba} represents the net flux of soluble surfactant that characterizes the mass exchange between the bulk and liquid film surface. Then J_{ba} can be expressed as [63,64]

$$J_{ba} = k_a(1 - \Gamma/\Gamma_\infty)c_b - k_d\Gamma, \quad (\text{A7})$$

where Γ_∞ is the surface surfactant concentration at maximum packing, and k_a and k_d are the absorption and desorption rate constants, respectively. At the film surface, $y = h(x, t)$, the net flux of soluble surfactant can also be described by the following Fickian diffusion [63]

$$J_{ba} = \frac{D_b}{\sqrt{1 + (\partial_x h)^2}} (\partial_x h \partial_x c_b - \partial_y c_b). \quad (\text{A8})$$

Finally, no mass flux condition at the inclined impermeable plane, $y = 0$, requires

$$\partial_y c_b = 0. \quad (\text{A9})$$

Since the surface tension σ changes with both the surface surfactant concentration Γ and temperature T , we will consider its linear variation as given in Eq. (2). The other boundary conditions at the liquid film surface, $y = h(x, t)$, are the same as provided in Eqs. (8)–(10), and (12). As our aim is to reproduce the results of D'Alessio *et al.* [27] in the limit $\tau_s \rightarrow 0$, we have preferred the same characteristic scales as suggested by them to nondimensionalize the governing equations. Then we can write

$$\begin{aligned} u^* &= \frac{du}{Q}, & v^* &= \frac{dv}{Q}, & p^* &= \frac{pd^2}{\rho Q^2}, & c_b^* &= \frac{dc_b}{\Gamma_\infty}, \\ x^* &= \frac{x}{d}, & y^* &= \frac{y}{d}, & h^* &= \frac{h}{d}, & \Gamma^* &= \frac{\Gamma}{\Gamma_\infty}, \\ t^* &= \frac{tQ}{d^2}, & \sigma^* &= \frac{\sigma}{\sigma_a}, & T^* &= \frac{T - T_a}{T_w - T_a}, & \tau &= \frac{\tau_s d^2}{\mu Q}, \end{aligned} \quad (\text{A10})$$

where $Q = \frac{\rho g \sin \theta d^3}{3\mu}$ is the flow rate for the steady unidirectional parallel flow with a constant film thickness d without imposed shear stress at the film surface. On the basis of the above characteristic scales, we can write the nondimensional governing equations and the associated boundary conditions as follows:

$$\partial_x u + \partial_y v = 0, \quad (\text{A11})$$

$$\text{Re}(\partial_t u + u \partial_x u + v \partial_y u + \partial_x p) = (\partial_{xx} u + \partial_{yy} u) + 3, \quad (\text{A12})$$

$$\text{Re}(\partial_t v + u \partial_x v + v \partial_y v + \partial_y p) = (\partial_{xx} v + \partial_{yy} v) - 3 \cot \theta, \quad (\text{A13})$$

$$\text{Pe}_T(\partial_t T + u \partial_x T + v \partial_y T) = (\partial_{xx} T + \partial_{yy} T), \quad (\text{A14})$$

$$\text{Pe}_B(\partial_t c_b + u \partial_x c_b + v \partial_y c_b) = (\partial_{xx} c_b + \partial_{yy} c_b), \quad (\text{A15})$$

$$u = 0, \quad v = 0, \quad T = 1, \quad \partial_y c_b = 0, \quad \text{at } y = 0, \quad (\text{A16})$$

$$[4\partial_y v \partial_x h + (\partial_y u + \partial_x v)\{1 - (\partial_x h)^2\}] + [\text{Re} M_2(\partial_x T + \partial_x h \partial_y T) + \text{Re} M_1 \partial_x \Gamma - \tau] \sqrt{1 + (\partial_x h)^2} = 0, \quad \text{at } y = h, \quad (\text{A17})$$

$$\text{Re}(p_a - p) + \frac{2}{[1 + (\partial_x h)^2]} \{\partial_y v [1 - (\partial_x h)^2] - \partial_x h (\partial_y u + \partial_x v)\} = \text{Re}[\text{We} - M_2 T - M_1(\Gamma - \Gamma_E)] \frac{\partial_{xx} h}{[1 + (\partial_x h)^2]^{3/2}}, \quad \text{at } y = h, \quad (\text{A18})$$

$$\frac{(\partial_x T \partial_x h - \partial_y T)}{\sqrt{1 + (\partial_x h)^2}} = \text{Bi} T, \quad \text{at } y = h, \quad (\text{A19})$$

$$\frac{(\partial_x h \partial_x c_b - \partial_y c_b)}{\text{Pe}_B \sqrt{1 + (\partial_x h)^2}} = k_s [\xi_s (1 - \Gamma) c_b - \Gamma], \quad \text{at } y = h, \quad (\text{A20})$$

$$\partial_t \Gamma + u \partial_x \Gamma + \frac{\Gamma}{1 + (\partial_x h)^2} [\partial_x u + \partial_x h \partial_x v + \partial_x h (\partial_y u + \partial_x h \partial_y v)] = \frac{1}{\text{Pe}_S \sqrt{1 + (\partial_x h)^2}} \partial_x \left[\frac{\partial_x \Gamma}{\sqrt{1 + (\partial_x h)^2}} \right] + k_s [\xi_s (1 - \Gamma) c_b - \Gamma], \quad \text{at } y = h, \quad (\text{A21})$$

$$\partial_t h + u \partial_x h = v, \quad \text{at } y = h, \quad (\text{A22})$$

where $\text{Re} = \frac{\rho Q}{\mu}$ is the Reynolds number, $\text{Pe}_T = \frac{\rho c_p Q}{\kappa}$ is the thermal Péclet number, $\text{Pe}_B = \frac{Q}{D_b}$ is the solutal Péclet number, $\text{Pe}_S = \frac{Q}{D_s}$ is the surfactant Péclet number, $\text{We} = \frac{\sigma_a d}{\rho Q^2}$ is the Weber number, $\text{Bi} = \frac{\lambda d}{\kappa}$ is the Biot number, $M_1 = \frac{E \Gamma_{\infty} d}{\rho Q^2}$ is the surfactant Marangoni number, $M_2 = \frac{\beta(T_w - T_a) d}{\rho Q^2}$ is the thermal Marangoni number, $k_s = \frac{k_a d^2}{Q}$, $\xi_s = \frac{k_a}{k_j d}$, and $\Gamma_E = \frac{\Gamma_a}{\Gamma_{\infty}}$. For our convenience, we have dropped the star notation from the nondimensional variables. For the linear stability analysis of the steady unidirectional parallel flow, we need its solution, which can be expressed as follows:

$$\bar{U}(y) = (3 + \tau)y - \frac{3}{2}y^2, \quad \bar{V}(y) = 0, \quad 0 \leq y \leq 1, \quad (\text{A23})$$

$$\bar{P}(y) = \frac{3 \cot \theta}{\text{Re}} (1 - y) + p_a, \quad \bar{H} = 1, \quad 0 \leq y \leq 1, \quad (\text{A24})$$

$$\bar{T}(y) = 1 - \left(\frac{\text{Bi}}{1 + \text{Bi}} \right) y, \quad \bar{\Gamma} = \Gamma_E, \quad \bar{c}_b = \frac{\Gamma_E}{\xi_s (1 - \Gamma_E)} = c_E, \quad 0 \leq y \leq 1, \quad (\text{A25})$$

where Γ_E and c_E are constants. Clearly, the range of Γ_E will be $0 < \Gamma_E < 1$. Moreover, we see that the surfactant concentration, \bar{c}_b , in the bulk vanishes when $\xi_s (1 - \Gamma_E) \rightarrow \infty$, which indicates the limiting situation of film flowing down a heated inclined plane with an insoluble surfactant at the surface.

1. Linear stability analysis

To study the primary instability of the steady unidirectional parallel flow, we apply an infinitesimal disturbance on the flat film flow of thickness $\bar{H} = 1$. Then, mathematically, we can write

$$u = \bar{U} + u', \quad v = \bar{V} + v', \quad p = \bar{P} + p', \quad T = \bar{T} + T', \quad h = \bar{H} + h', \\ \Gamma = \bar{\Gamma} + \Gamma', \quad c_b = \bar{c}_b + c'_b, \quad (\text{A26})$$

where prime quantities represent the perturbation variables. Next, we follow the same procedure as described in Sec. III. To develop the Orr-Sommerfeld-type boundary value problem, we assume the

solution of the linearized perturbation equations in the normal mode form:

$$\left. \begin{aligned} \psi'(x, y, t) &= \hat{\phi}(y) \exp[ik(x - ct)], \\ T'(x, y, t) &= \hat{T}(y) \exp[ik(x - ct)], \\ c'_b(x, y, t) &= \hat{c}_b(y) \exp[ik(x - ct)], \\ \Gamma'(x, t) &= \hat{\Gamma} \exp[ik(x - ct)], \\ h'(x, t) &= \hat{\eta} \exp[ik(x - ct)], \end{aligned} \right\} \quad (\text{A27})$$

in which hat quantities specify the amplitudes of the perturbation variables. Inserting Eq. (A27) in the linearized perturbation equations, and after some mathematical calculations, one can derive the following form of the Orr-Sommerfeld-type boundary value problem:

$$(D^2 - k^2)^2 \hat{\phi} = ik \text{Re}[(\bar{U} - c)(D^2 - k^2) - D^2 \bar{U}] \hat{\phi}, \quad 0 \leq y \leq 1, \quad (\text{A28})$$

$$(D^2 - k^2) \hat{T} = ik \text{Pe}_T [(\bar{U} - c) \hat{T} - D \bar{T} \hat{\phi}], \quad 0 \leq y \leq 1, \quad (\text{A29})$$

$$(D^2 - k^2) \hat{c}_b = ik \text{Pe}_B (\bar{U} - c) \hat{c}_b, \quad 0 \leq y \leq 1, \quad (\text{A30})$$

$$\hat{\phi} = 0, \quad \hat{T} = 0, \quad D \hat{\phi} = 0, \quad D \hat{c}_b = 0, \quad \text{at } y = 0, \quad (\text{A31})$$

$$(D^2 + k^2) \hat{\phi} + ik \text{Re} M_2 (\hat{T} + D \bar{T} \hat{\eta}) + ik \text{Re} M_1 \hat{\Gamma} + D^2 \bar{U} \hat{\eta} = 0, \quad \text{at } y = 1, \quad (\text{A32})$$

$$\begin{aligned} (D^3 - 3k^2 D) \hat{\phi} - ik \text{Re} [(\bar{U} - c) D \hat{\phi} - D \bar{U} \hat{\phi}] \\ = ik \hat{\eta} [k^2 \text{Re}(\text{We} - M_2 \bar{T}) - \text{Re} D \bar{P} - 2ik D \bar{U}], \quad \text{at } y = 1, \end{aligned} \quad (\text{A33})$$

$$D \hat{T} + \text{Bi} [\hat{T} + D \bar{T} \hat{\eta}] = 0, \quad \text{at } y = 1, \quad (\text{A34})$$

$$D \hat{c}_b + \text{Pe}_B k_s [\xi_s (1 - \Gamma_E) \hat{c}_b - (1 + \xi_s \bar{c}_b) \hat{\Gamma}] = 0, \quad \text{at } y = 1, \quad (\text{A35})$$

$$ik(\bar{U} - c) \hat{\Gamma} + ik \Gamma_E [D \hat{\phi} + D \bar{U} \hat{\eta}] = -\frac{k^2}{\text{Pe}_S} \hat{\Gamma} + k_s [\xi_s (1 - \Gamma_E) \hat{c}_b - (1 + \xi_s \bar{c}_b) \hat{\Gamma}], \quad \text{at } y = 1, \quad (\text{A36})$$

$$\hat{\phi} + (\bar{U} - c) \hat{\eta} = 0, \quad \text{at } y = 1. \quad (\text{A37})$$

It should be useful to mention here that the Orr-Sommerfeld-type boundary value problem (A28)–(A37) coincides with that of D'Alessio *et al.* [27] in the absence of imposed shear stress if we ignore their printing mistakes present in Eqs. (3.2) and (3.5).

2. Long-wave analytical solution

To explore the temporal stability analysis, we follow the same technique as described in Sec. III. As a result, we expand the variables $\hat{\phi}$, \hat{T} , \hat{c}_b , $\hat{\eta}$, $\hat{\Gamma}$, and c as the sum of infinite series in the limit $k \rightarrow 0$

$$\left. \begin{aligned} \hat{\phi}(y) &= \sum_{n=0}^{\infty} \phi_n k^n, & \hat{T}(y) &= \sum_{n=0}^{\infty} T_n k^n, & \hat{c}_b &= \sum_{n=0}^{\infty} c_{bn} k^n, \\ \hat{\eta} &= \sum_{n=0}^{\infty} \eta_n k^n, & \hat{\Gamma} &= \sum_{n=0}^{\infty} \Gamma_n k^n, & c &= \sum_{n=0}^{\infty} c_n k^n. \end{aligned} \right\} \quad (\text{A38})$$

After substituting the long-wave expansion (A38) in the Orr-Sommerfeld-type boundary value problem (A28)–(A37), we collect the zeroth-order [$O(k^0)$] equations:

$$D^4\phi_0(y) = 0, \quad D^2T_0(y) = 0, \quad D^2c_{b0}(y) = 0, \quad 0 \leq y \leq 1, \quad (\text{A39})$$

$$\phi_0(y) = 0, \quad T_0(y) = 0, \quad D\phi_0(y) = 0, \quad Dc_{b0}(y) = 0, \quad \text{at } y = 0, \quad (\text{A40})$$

$$D^2\phi_0(y) + D^2\bar{U}(y)\eta_0 = 0, \quad D^3\phi_0(y) = 0, \quad \text{at } y = 1, \quad (\text{A41})$$

$$DT_0(y) + Bi T_0(y) + Bi D\bar{T}(y)\eta_0 = 0, \quad \text{at } y = 1, \quad (\text{A42})$$

$$Dc_{b0}(y) + Pe_B k_s[\xi_s(1 - \Gamma_E)c_{b0}(y) - (1 + \xi_s\bar{c}_b)\Gamma_0] = 0, \quad \text{at } y = 1, \quad (\text{A43})$$

$$k_s[\xi_s(1 - \Gamma_E)c_{b0}(y) - (1 + \xi_s\bar{c}_b)\Gamma_0] = 0, \quad \text{at } y = 1, \quad (\text{A44})$$

$$\phi_0(y) + (\bar{U}(y) - c_0)\eta_0 = 0, \quad \text{at } y = 1. \quad (\text{A45})$$

Solving the zeroth-order equations (A39)–(A44), we can write the solution in the following form:

$$\phi_0(y) = \frac{3\eta_0 y^2}{2}, \quad T_0(y) = \frac{Bi^2\eta_0 y}{(1 + Bi)^2}, \quad \text{and} \quad c_{b0} = \frac{(1 + \xi_s c_E)\Gamma_0}{\xi_s(1 - \Gamma_E)}. \quad (\text{A46})$$

Finally, plugging the zeroth-order solution into the kinematic boundary condition (A45), one can get the phase speed of the surface mode

$$c_0 = c_{0s} = (3 + \tau), \quad (\text{A47})$$

provided $\eta_0 \neq 0$. In the long-wave calculation, we are concerned only with the surface mode. Next, we collect the first-order [$O(k^1)$] equations, which are given below:

$$D^4\phi_1(y) + i \operatorname{Re}\{D^2\bar{U}(y)\phi_0(y) + [c_0 - \bar{U}(y)]D^2\phi_0(y)\} = 0, \quad 0 \leq y \leq 1, \quad (\text{A48})$$

$$D^2T_1(y) + i \operatorname{Pe}_T\{D\bar{T}(y)\phi_0(y) + [c_0 - \bar{U}(y)]T_0(y)\} = 0, \quad 0 \leq y \leq 1, \quad (\text{A49})$$

$$D^2c_{b1}(y) + i \operatorname{Pe}_B[c_0 - \bar{U}(y)]c_{b0} = 0, \quad 0 \leq y \leq 1, \quad (\text{A50})$$

$$\phi_1(y) = 0, \quad T_1(y) = 0, \quad D\phi_1(y) = 0, \quad Dc_{b1}(y) = 0, \quad \text{at } y = 0, \quad (\text{A51})$$

$$D^2\phi_1(y) + i \operatorname{Re} M_2[T_0(y) + D\bar{T}(y)\eta_0] + i \operatorname{Re} M_1\Gamma_0 + D^2\bar{U}(y)\eta_1 = 0, \quad \text{at } y = 1, \quad (\text{A52})$$

$$D^3\phi_1(y) + i \operatorname{Re}\{[c_0 - \bar{U}(y)]D\phi_0(y) + D\bar{U}(y)\phi_0(y) + D\bar{P}(y)\eta_0\} = 0, \quad \text{at } y = 1, \quad (\text{A53})$$

$$DT_1(y) + Bi[T_1(y) + D\bar{T}(y)\eta_1] = 0, \quad \text{at } y = 1, \quad (\text{A54})$$

$$Dc_{b1}(y) + Pe_B k_s[\xi_s(1 - \Gamma_E)c_{b1}(y) - (1 + \xi_s\bar{c}_b)\Gamma_1] = 0, \quad \text{at } y = 1, \quad (\text{A55})$$

$$i[\bar{U}(y) - c_0]\Gamma_0 + i\Gamma_E[D\phi_0(y) + D\bar{U}(y)\eta_0] - k_s[\xi_s(1 - \Gamma_E)c_{b1} - (1 + \xi_s\bar{c}_b)\Gamma_1] = 0, \quad \text{at } y = 1, \quad (\text{A56})$$

$$\phi_1(y) - [c_0 - \bar{U}(y)]\eta_1 - c_1\eta_0 = 0, \quad \text{at } y = 1. \quad (\text{A57})$$

First, we have solved the convection-diffusion equation (A50) for soluble surfactant in the bulk, which leads to

$$\Gamma_0 = \frac{2(3 + \tau)\Gamma_E \xi_s(1 - \Gamma_E)^2\eta_0}{4 + 3\xi_s(1 - \Gamma_E)^2 + \tau}. \quad (\text{A58})$$

Next, solving the equations for stream function and temperature and substituting their solution in the kinematic boundary condition (A59), we get

$$c_{1s} = i\text{Re} \left[\frac{6}{5} - \frac{\cot \theta}{\text{Re}} + \frac{M_2 \text{Bi}}{2(1 + \text{Bi})^2} - \frac{M_1(3 + \tau)\Gamma_E \xi_s(1 - \Gamma_E)^2}{4 + 3\xi_s(1 - \Gamma_E)^2 + \tau} + \frac{2}{5}\tau \right]. \quad (\text{A59})$$

Clearly, Eq. (A59) coincides with the expression of D'Alessio *et al.* [27] if the imposed shear stress is absent. As discussed by D'Alessio *et al.* [27], the result of surface mode for the thermocapillary instability in the presence of insoluble surface surfactant is recovered if $\xi_s(1 - \Gamma_E) \rightarrow \infty$ and $\tau \rightarrow 0$. In this limit, the expression (A59) becomes

$$c_{1s} = i\text{Re} \left[\frac{6}{5} - \frac{\cot \theta}{\text{Re}} + \frac{M_2 \text{Bi}}{2(1 + \text{Bi})^2} - M_1 \Gamma_E \right]. \quad (\text{A60})$$

Equation (A60) reveals that the temporal growth rate, $kc_{1s} \propto |c_{1s}|$ ($k \rightarrow 0$), intensifies if the thermal Marangoni number M_2 increases, while the temporal growth rate reduces if the surfactant Marangoni number M_1 increases. Hence, the long-wave analysis predicts similar results for the surface mode, as observed in the case of the heated film flow with an insoluble surfactant and without shear stress acting at the film surface.

-
- [1] K. Huang, Y. Hu, and X. Deng, Experimental study on heat and mass transfer of falling liquid films in converging-diverging tubes with water, *Int. J. Heat Mass Transfer* **126**, 721 (2018).
- [2] P. D. Frisk and E. J. Davis, The enhancement of heat transfer by waves in stratified gas-liquid flow, *Int. J. Heat Mass Transfer* **15**, 1537 (1972).
- [3] N. Brauner and D. M. Maron, Characteristics of inclined thin films, waviness and the associated mass transfer, *Int. J. Heat Mass Transfer* **25**, 99 (1982).
- [4] Y. He, P. Yazhgur, A. Salonen, and D. Langvein, Absorption-desorption kinetics of surfactants at liquid surfaces, *Adv. Colloid Interface Sci.* **222**, 377 (2015).
- [5] P. L. Kapitza and S. P. Kapitza, Wave flow of thin fluid layers of liquid, *Zh. Eksp. Teor. Fiz.* **19**, 105 (1949).
- [6] S. V. Alekseenko, V. Y. Nakoryakov, and B. G. Pokusaev, Wave formation on a vertical falling liquid film, *AIChE J.* **31**, 1446 (1985).
- [7] H. C. Chang, Wave evolution on a falling film, *Annu. Rev. Fluid Mech.* **26**, 103 (1994).
- [8] J. Liu and J. P. Gollub, Solitary wave dynamics of film flows, *Phys. Fluids* **6**, 1702 (1994).
- [9] T. B. Benjamin, Wave formation in laminar flow down an inclined plane, *J. Fluid Mech.* **2**, 554 (1957).
- [10] C. S. Yih, Stability of liquid flow down an inclined plane, *Phys. Fluids* **6**, 321 (1963).
- [11] S. P. Lin, Instability of a liquid film flowing down an inclined plane, *Phys. Fluids* **10**, 308 (1967).
- [12] G. J. De Bruin, Stability of a layer of liquid flowing down an inclined plane, *J. Eng. Math.* **8**, 259 (1974).
- [13] R. Chin, F. Abernathy, and J. Bertschy, Gravity and shear wave stability of free surface flows. Part 1. Numerical calculations, *J. Fluid Mech.* **168**, 501 (1986).
- [14] J. M. Floryan, S. H. Davis, and R. E. Kelly, Instabilities of a liquid film flowing down a slightly inclined plane, *Phys. Fluids* **30**, 983 (1987).
- [15] A. Samanta, Modal and nonmodal stability analysis for an electrified falling film, *Phys. Rev. E* **107**, 045105 (2023).
- [16] S. P. Lin, Stability of liquid flow down a heated inclined plane, *Lett. Heat Mass Trans.* **2**, 361 (1975).
- [17] S. Sreenivasan and S. P. Lin, Surface tension driven instability of a liquid film flow down a heated incline, *Int. J. Heat Mass Transf.* **21**, 1517 (1978).
- [18] M. K. Smith, The long-wave instability in heated or cooled inclined liquid layers, *J. Fluid Mech.* **219**, 337 (1990).

- [19] D. A. Goussis and R. E. Kelly, Surface wave and thermocapillary instabilities in a liquid film flow, *J. Fluid Mech.* **223**, 25 (1991).
- [20] S. W. Joo, S. H. Davis, and S. G. Bankoff, Long-wave instabilities of heated falling films: Two-dimensional theory of uniform layers, *J. Fluid Mech.* **230**, 117 (1991).
- [21] S. W. Joo, S. H. Davis, and S. G. Bankoff, A mechanism for rivulet formation in heated falling films, *J. Fluid Mech.* **321**, 279 (1996).
- [22] C. Ruyer-Quil, B. Scheid, S. Kalliadasis, M. G. Velarde, and R. K. Zeytounian, Thermocapillary long waves in a liquid film flow. Part 1. Low-dimensional formulation, *J. Fluid Mech.* **538**, 199 (2005).
- [23] B. Scheid, C. Ruyer-Quil, S. Kalliadasis, M. G. Velarde, and R. K. Zeytounian, Thermocapillary long waves in a liquid film flow. Part 2. Linear stability and nonlinear waves, *J. Fluid Mech.* **538**, 223 (2005).
- [24] J. Hu, H. B. Hadid, D. Henry, and A. Mojtabi, Linear temporal and spatiotemporal stability analysis of a binary liquid film flowing down an inclined uniformly heated plate, *J. Fluid Mech.* **599**, 269 (2008).
- [25] J. P. Pascal and S. J. D. D'Alessio, Thermosolutal Marangoni effects on the inclined flow of a binary liquid with variable density. I. Linear stability analysis, *Phys. Rev. Fluids* **1**, 083603 (2016).
- [26] S. J. D. D'Alessio and J. P. Pascal, Thermosolutal Marangoni effects on the inclined flow of a binary liquid with variable density. II. Nonlinear analysis and simulations, *Phys. Rev. Fluids* **1**, 083604 (2016).
- [27] S. D'Alessio, J. P. Pascal, E. Ellaban, and C. Ruyer-Quil, Marangoni instabilities associated with heated surfactant-laden falling films, *J. Fluid Mech.* **887**, A20 (2020).
- [28] A. Samanta, Stability of inertialess liquid film flowing down a heated inclined plane, *Phys. Lett. A* **372**, 6653 (2008).
- [29] L. A. Dávalos-Orozco, The effect of the thermal conductivity and thickness of the wall on the nonlinear instability of a thin film flowing down an incline, *Int. J. Non Linear Mech.* **47**, 1 (2012).
- [30] L. A. Dávalos-Orozco, Stability of thin liquid films falling down isothermal and non-isothermal walls, *Interfac. Phenom. Heat Transf.* **1**, 93 (2013).
- [31] A. Choudhury and A. Samanta, Linear stability of a falling film over a heated slippery plane, *Phys. Rev. E* **105**, 065112 (2022).
- [32] A. Choudhury and A. Samanta, Thermocapillary instability for a shear-imposed falling film, *Phys. Rev. Fluids* **8**, 094006 (2023).
- [33] S. Whitaker and L. O. Jones, Stability of falling liquid films: Effect of interface and interfacial mass transport, *AIChE J.* **12**, 421 (1966).
- [34] M. G. Blyth and C. Pozrikidis, Effect of surfactant on the stability of film flow down an inclined plane, *J. Fluid Mech.* **521**, 241 (2004).
- [35] H. H. Wei, Effect of surfactant on the long-wave instability of a shear-imposed liquid flow down an inclined plane, *Phys. Fluids* **17**, 012103 (2005).
- [36] F. A. Bhat and A. Samanta, Linear stability analysis of a surfactant-laden shear-imposed falling film, *Phys. Fluids* **31**, 054103 (2019).
- [37] A. L. Frenkel and D. Halpern, Stokes-flow instability due to interfacial surfactant, *Phys. Fluids* **14**, L45 (2002).
- [38] A. Samanta, Effect of surfactant on two-layer channel flow, *J. Fluid Mech.* **735**, 519 (2013).
- [39] S. D'Alessio and J. P. Pascal, Long-wave instability in thin heated films doped with soluble surfactants, *Int. J. Non Linear Mech.* **136**, 103784 (2021).
- [40] R. T. van Gaalen, H. M. A. Wijshoff, J. G. M. Kuerten, and C. Diddens, Competition between thermal and surfactant-induced Marangoni flow in evaporating sessile droplets, *J. Colloid Interface Sci.* **622**, 892 (2022).
- [41] S. Kalliadasis, C. Ruyer-Quil, B. Scheid, and M. G. Velarde, *Falling Liquid Films* (Springer, Berlin, 2012).
- [42] S. Miladinova, S. Slavtchev, G. Lebon, and J. C. Legros, Long-wave instabilities of non-uniformly heated falling films, *J. Fluid Mech.* **453**, 153 (2002).
- [43] A. Samanta, Stability of liquid film falling down a vertical non-uniformly heated wall, *Physica D* **237**, 2587 (2008).
- [44] D. Halpern and A. L. Frenkel, Destabilization of a creeping flow by interfacial surfactant: Linear theory extended to all wavenumbers, *J. Fluid Mech.* **485**, 191 (2003).

- [45] A. Samanta, Effect of surfactants on the instability of a two-layer film flow down an inclined plane, *Phys. Fluids* **26**, 094105 (2014).
- [46] F. A. Bhat and A. Samanta, Linear stability for surfactant-laden two-layer film flows down a slippery inclined plane, *Chem. Eng. Sci.* **220**, 115611 (2020).
- [47] A. Samanta, Linear stability of a plane Couette-Poiseuille flow overlying a porous layer, *Int. J. Multiphase Flow* **123**, 103160 (2020).
- [48] P. M. J. Trevelyan and S. Kalliadasis, Wave dynamics on a thin-liquid film falling down a heated wall, *J. Eng. Math.* **50**, 177 (2004).
- [49] F. A. Bhat and A. Samanta, Linear stability of a contaminated fluid flow down a slippery inclined plane, *Phys. Rev. E* **98**, 033108 (2018).
- [50] A. Samanta, Shear-imposed falling film, *J. Fluid Mech.* **753**, 131 (2014).
- [51] A. Samanta, Optimal disturbance growth in shear-imposed falling film, *AIChE J.* **66**, e16906 (2020).
- [52] A. Samanta, Spatiotemporal instability of a shear-imposed viscous flow, *Phys. Fluids* **33**, 094104 (2021).
- [53] A. Samanta, Effect of surfactant on the linear stability of a shear-imposed fluid flowing down a compliant substrate, *J. Fluid Mech.* **920**, A23 (2021).
- [54] U. Lange, K. Nandakumar, and H. Raszillier, Symbolic computation as a tool for high-order long-wave stability analysis of thin film flows with coupled transport processes, *J. Comput. Phys.* **150**, 1 (1999).
- [55] S. Pal and A. Samanta, Linear stability of a surfactant-laden viscoelastic liquid flowing down a slippery inclined plane, *Phys. Fluids* **33**, 054101 (2021).
- [56] P. Schmid and D. Henningson, *Stability and Transition in Shear Flows* (Springer, Berlin, 2001).
- [57] A. Samanta, Shear wave instability for electrified falling films, *Phys. Rev. E* **88**, 053002 (2013).
- [58] P. Huerre and P. A. Monkewitz, Local and global instabilities in spatially developing flows, *Annu. Rev. Fluid Mech.* **22**, 473 (1990).
- [59] A. Samanta, Spatiotemporal instability of an electrified falling film, *Phys. Rev. E* **93**, 013125 (2016).
- [60] W. Ji and F. Setterwall, On the instabilities of vertical falling liquid films in the presence of surface-active solute, *J. Fluid Mech.* **278**, 297 (1994).
- [61] G. Karapetsas and V. Bontozoglou, The role of surfactants on the mechanism of the long-wave instability in liquid film flows, *J. Fluid Mech.* **741**, 139 (2014).
- [62] A. Pereira and S. Kalliadasis, On the transport equation for an interfacial quantity, *Eur. Phys. J. Appl. Phys.* **44**, 211 (2011).
- [63] A. Nepomnyaschy, M. G. Velarde, and P. Colinet, *Interfacial Phenomena and Convection* (CRC Press, New York, 2002).
- [64] B. D. Edmonstone, R. V. Craster, and O. K. Matar, Surfactant-induced fingering phenomena beyond the critical micelle concentration, *J. Fluid Mech.* **564**, 105 (2006).